Submitted to the Astrophysical Journal
Preprint typeset using LaTeX style emulateapj v. 6/22/04



# A CHANDRA VIEW OF DARK MATTER IN EARLY-TYPE GALAXIES

Philip J. Humphrey[1], David A. Buote[1], Fabio Gastaldello[1], Luca Zappacosta[1], James S. Bullock[1], Fabrizio Brighenti[2,3] and William G. Mathews[3]

*Submitted to the Astrophysical Journal*

## ABSTRACT

We present a *Chandra* study of mass profiles in 7 elliptical galaxies, of which 3 have galaxy-scale and 4 group-scale halos, demarcated at $10^{13}M_{\odot}$. These represent the best available data for nearby objects with comparable X-ray luminosities. We measure ∼flat mass-to-light (M/L) profiles within an optical half-light radius ($R_{\rm eff}$), rising by an order of magnitude at $\sim 10R_{\rm eff}$, which confirms the presence of dark matter (DM). The data indicate hydrostatic equilibrium, which is also supported by agreement with studies of stellar kinematics in elliptical galaxies. The data are well-fitted by a model comprising an NFW DM profile and a baryonic component following the optical light. The distribution of DM halo concentration parameters (c) *versus* $M_{\rm vir}$ agrees with ΛCDM predictions and our observations of bright groups. Concentrations are slightly higher than expected, which is most likely a selection effect. Omitting the stellar mass drastically increases c, possibly explaining large concentrations found by some past observers. The stellar $M/L_K$ agree with population synthesis models, assuming a Kroupa IMF. Allowing adiabatic compression (AC) of the DM halo by baryons made M/L more discrepant, casting some doubt on AC. Our best-fitting models imply total baryon fractions ∼0.04–0.09, consistent with models of galaxy formation incorporating strong feedback. The groups exhibit positive temperature gradients, consistent with the "Universal" profiles found in other groups and clusters, whereas the galaxies have negative gradients, suggesting a change in the evolutionary history of the systems around $M_{\rm vir} \simeq 10^{13}M_{\odot}$.

*Subject headings:* Xrays: galaxies— galaxies: elliptical and lenticular, cD— galaxies: halos— galaxies: ISM— dark matter

## 1. INTRODUCTION

The nature and distribution of dark matter (DM) in the Universe is one of the fundamental problems facing modern physics. Cold DM lies at the heart of our current (ΛCDM) cosmological paradigm, which predicts substantial DM halos for objects at all mass-scales from galaxies to clusters. Although ΛCDM has been remarkably successful at explaining large-scale features (e.g. Spergel et al. 2003; Perlmutter et al. 1999), observations of galaxies have been more problematical for the theory. Dissipationless dark matter simulations find that dark matter halos are well characterized by a "Universal" mass density profile (Navarro et al. 1997, hereafter NFW) over a wide range of Virial masses ($M_{\rm vir}$) (e.g. Bullock et al. 2001). Low mass halos tend to form first in hierarchical cosmologies and are consequently more tightly concentrated than their later forming, high mass counterparts. This tendency produces a predicted correlation between the DM halo concentration parameter (c, which is ratio between Virial radius, $R_{\rm vir}$, and the characteristic scale of the density profile) and $M_{\rm vir}$(Navarro et al. 1997). However, since mass and formation epoch are not perfectly correlated, we expect a significant scatter at fixed Virial mass (Jing 2000; Bullock et al. 2001; Wechsler et al. 2002). The tight link between halo formation epoch and concentration implies that the precise relation between c and $M_{\rm vir}$ is sensitive to the underlying Cosmological parameters, including $\sigma_8$ and the dark energy equation of state (Kuhlen et al. 2005), making an observational test of this relation potentially a very powerful tool for cosmology.

The mass profiles of galaxies also may provide valuable clues as to the way in which galaxies form in DM halos. In particular, as baryons cool and collapse into stars, the associated increase in the central mass density should in turn modify the shape of the DM halo. This process is typically modelled assuming adiabatic contraction (AC) of the DM particle orbits (e.g. Blumenthal et al. 1986; Gnedin et al. 2004). If the galaxy halo subsequently evolves by major mergers, simulations are unclear as to whether these features would persist (e.g. Gnedin et al. 2004) or whether the merging process may destroy this imprint of star formation, or even mix the DM and baryons sufficiently to produce a *total* gravitating mass profile more akin to NFW (Loeb & Peebles 2003; El-Zant et al. 2004).

Observational tests of the predictions of ΛCDM have proven controversial. In clusters of galaxies there is overwhelming evidence for DM, and an increasing body of work verifying the predictions of ΛCDM. In particular recent, high-quality *Chandra* and *XMM* observations have revealed mass profiles in remarkable agreement with the Universal profile from deep in the core to a large fraction of $R_{\rm vir}$ (e.g. Lewis et al. 2003; Zappacosta et al. 2006; Vikhlinin et al. 2005), and a distribution of c *versus* $M_{\rm vir}$ in good agreement with ΛCDM (Pointecouteau et al. 2005). In galaxies, however, the picture is much less clear. Rotation curve analysis of low surface brightness (LSB) disk galaxies has suggested significantly less cuspy density profiles than expected (e.g. Swaters et al. 2000).

[1] Department of Physics and Astronomy, University of California at Irvine, 4129 Frederick Reines Hall, Irvine, CA 92697-4575
[2] Dipartimento di Astronomia, Università di Bologna, Via Ranzani 1, Bologna 40127, Italy
[3] University of California Observatories, Lick Observatory, University of California at Santa Cruz, Santa Cruz, CA 95064

Although this discrepancy led to a serious discussion of modifications to the standard paradigm (e.g. Hogan & Dalcanton 2000; Spergel & Steinhardt 2000; Zentner & Bullock 2002; Kaplinghat 2005; Cembranos et al. 2005), recent results, taking account of observational bias and the 3-dimensional geometry of the DM halos, have done much to resolve the discrepancy (e.g. Swaters et al. 2003; Simon et al. 2005). However, some significant discrepancies remain, not least of which is that the DM halos of these galaxies appear less concentrated than expected (e.g. Gonzalez et al. 2000; Kassin et al. 2006). A possible explanation is that LSB galaxies are preferentially found in low-concentration halos (Bullock et al. 2001; Bailin et al. 2005; Wechsler et al. 2005), making additional constraints at the galaxy scale extremely important.

In many respects, kinematical mass measurements are far more challenging for early-type than spiral galaxies. As essentially pressure-supported systems little is known *a priori* about the velocity anisotropy tensor of the stars in elliptical galaxies, which is problematical for the determination of the mass from stellar motions. Nonetheless, stellar kinematical measurements have widely been used as a means to measure the gravitating matter within ∼the optical half-light radius ($R_{\rm eff}$) of elliptical galaxies (e.g. Binney et al. 1990; van der Marel 1991; Gerhard et al. 2001). These studies tend to find relatively flat mass-to-light (M/L) ratios within $R_{\rm eff}$, implying that most of the matter within this radius is baryonic. Consideration of the tilt in the fundamental plane can also lead to the same conclusion (Borriello et al. 2003). In contrast, Padmanabhan et al. (2004) pointed out that dynamical M/L ratios within $R_{\rm eff}$ are much larger than predicted by realistic stellar population synthesis models for stars alone, allowing $\gtrsim 50\%$ of the mass within $R_{\rm eff}$ to be dark.

Attempts to extend kinematical studies of elliptical galaxies to larger radii, where DM should be dominant, have proven controversial. In particular Romanowsky et al. (2003) argued against the existence of DM in a small sample of elliptical galaxies, based on planetary nebulae dynamics within $\sim 5R_{\rm eff}$. We note that this sample was heavily biased towards very X-ray faint objects, which might hint at low-mass halos since they have not held onto their hot gas. In any case Dekel et al. (2005) pointed out that their conclusions were very sensitive to the uncertainty in the velocity anisotropy tensor, for plausible values of which the data were consistent with substantial DM halos. In fact globular cluster dynamics in one of these systems, NGC 3379, does imply a significant amount of DM (Pierce et al. 2006; Bergond et al. 2006). As more kinematical studies of early-type galaxies at large radii are appearing, it is becoming clear that at least some elliptical galaxies host considerable DM halos (e.g. Statler et al. 1999; Romanowsky 2005). There persist some questions, however, as to the extent to which all galaxies have DM halos consistent with ΛCDM. In particular Napolitano et al. (2005) argued that a substantial number of early-type galaxy halos appear less concentrated than expected.

Gravitational lensing provides further evidence that, at least some, early-type galaxies possess substantial DM halos (e.g. Kochanek 1995; Fischer et al. 2000; Rusin et al. 2002). Since weak lensing of galaxies only provides useful mass constraints in a statistical sense, the relatively rare instances of strong lensing are required to study DM in individual systems. Nonetheless it has been possible in a few cases to decompose the mass into stellar and DM components, albeit with strong assumptions or additional observational constraints (e.g. Rusin et al. 2003; Treu & Koopmans 2004).

X-ray observations of the hot gas in early-type galaxies provide a complementary means to infer the mass-profiles *via* techniques similar to those used in studying clusters. Since the X-ray emission from early-type galaxies is typically not very bright, prior to the advent of *Chandra* and *XMM* this was limited by the relatively sparse information on the radial temperature and density profiles of the hot gas which could be determined by prior generations of satellites. Notwithstanding this limitation, large M/L ratios (consistent with substantial DM) were inferred for a number of X-ray bright galaxies, albeit with strong assumptions concerning the temperature and density profiles (e.g. Forman et al. 1985; Loewenstein & White 1999). Using a novel technique which relied, instead, on the ellipticity of the X-ray halo, Buote & Canizares (1994) were able robustly to detect DM in the isolated elliptical NGC 720 (see also Buote & Canizares 1996, 1998; Buote et al. 2002). Detailed measurements of the radial mass distribution were, however, largely restricted to a few massive systems, which may be entwined with a group halo (e.g. Irwin & Sarazin 1996; Brighenti & Mathews 1997). Nevertheless Brighenti & Mathews (1997) were able to decompose the mass profiles of two systems, NGC 4472 and NGC 4649, into stellar and DM components. Sato et al. (2000) investigated the $M_{\rm vir}$-c relation using *ASCA* for a sample of objects ranging from massive clusters to ∼3 elliptical galaxies. The limited spatial resolution of *ASCA* necessitated some assumptions about the density profiles and, crucially, the authors neglected any stellar mass component in their fits. This omission may explain the very steep $M_{\rm vir}$-c relation (with $c_{200} \gtrsim 30$ for the galaxies) found by these authors, in conflict with ΛCDM (Mamon & Łokas 2005).

Although mass profiles of early-type galaxies are beginning to appear which exploit the improved sensitivity and resolution of *Chandra* and *XMM*, many of the most interesting constraints on DM are still restricted to massive systems, which may be at the centres of groups. For example, Fukazawa et al. (2006) reported *Chandra* and *XMM* M/L profiles for ∼50 galaxies and groups, confirming ∼flat profiles within $R_{\rm eff}$ which rise at larger radii. However, the constraints at large radii were dominated by the massive (group-scale) objects so the implications for the DM content of normal galaxies are unclear. Furthermore, the authors included a substantial number of highly disturbed systems, in which hydrostatic equilibrium may be questioned, and failed to account for the unresolved sources which dominate the emission in the lowest-$L_X$ objects in their sample[4]. Recently, however, detailed *Chandra* and *XMM* mass profiles have begun to appear for isolated early-type galaxies, also confirming the presence of massive DM halos (e.g. O'Sullivan & Ponman 2004; Khosroshahi et al. 2004).

This paper is part of a series (see also Gastaldello et al.

[4] Although the authors account for unresolved sources when measuring the gas temperature, they do not account for it when computing the gas density, where its effect is more pronounced

2006; Zappacosta et al. 2006; Buote et al. 2006a,b) using high-quality *Chandra* and *XMM* data to investigate the mass profiles of galaxies, groups and clusters. This provides an unprecedented opportunity to place definitive constraints upon the $M_{vir}$-c relation over $\sim$2 orders of magnitude in $M_{vir}$. In this paper, we focus on the temperature, density and mass profiles of seven galaxies and poor groups chosen from the *Chandra* archive. In order to compare to theory we perform spherically-averaged analysis, leaving a discussion of the ellipticities of the X-ray halos to a future paper. In § 2 we discuss the target selection. The data-reduction is described in § 3 and the X-ray morphology is addressed in § 4. We discuss the spectral analysis in § 5, the mass analysis in § 6, the systematic uncertainties in our analysis in § 7 and reach our conclusions in § 8. The three systems for which we find $M_{vir} < 10^{13} M_\odot$ are optically isolated and so we refer to them as "galaxies", and the other systems in our sample as groups. We discuss this in more detail in § 8.3. In this paper, all error-bars quoted represent 90% confidence limits, unless otherwise stated, and we computed Virial quantities assuming a "critical overdensity" factor for the DM halos of $\rho_{halo}/\rho_{crit} = 103$ (where $\rho_{halo}$ is the mean density of a sphere of mass $M_{vir}$ and radius $R_{vir}$).

## 2. TARGET SELECTION

We chose, for this initial study, to focus on objects observed with *Chandra*. *Chandra* data are particularly valuable for the study of galaxies since the unprecedented spatial resolution makes it possible to resolve the temperature and density profiles deep into the galaxy core, allowing us to disentangle the stellar and dark matter, and resolve them into discrete components. We initially chose a set of potential target systems from detections listed in the X-ray catalogue of O'Sullivan et al. (2001) which have non-grating ACIS data in the *Chandra* archive. To eliminate bright groups and cluster cDs in the sample, we excluded galaxies with $L_X \gtrsim 10^{43}$erg s$^{-1}$. In order to perform the required spatially-resolved spectroscopy, we required at least $\sim$5000 hot gas photons. The potential targets were processed and the 0.1–10.0 keV image examined for evidence of large-scale disturbances (§ 4). We included some systems with low-amplitude asymmetries which should not strongly disturb hydrostatic equilibrium (we discuss this in more detail in § 7.4). Preliminary analysis was conducted to estimate the Virial mass of the object (§ 6). Since we aimed to focus on lower-mass objects, systems for which a fit using a simple NFW profile yielded $M_{vir} \gtrsim 10^{13} M_\odot$were discounted. Massive objects of this type are the focus of another study (Gastaldello et al. 2006). The most promising candidates for study found *via* this method were chosen for detailed analysis. The properties of the 7 objects in our sample and the *Chandra* exposures are shown in Table 1.

Our selection criteria naturally bias the sample towards X-ray bright galaxies. One might expect that galaxies sitting in deep potential wells are more likely to retain hot gas than those with little dark matter, and so our results may be biased somewhat towards those galaxies with substantial dark halos (in contrast to the opposite bias in the analysis of Romanowsky et al. 2003). As we are selecting objects which are not heavily disturbed, we are also biased towards galaxies which have not recently undergone a major merger. For the purposes of this paper, however, we do not require statistical completeness, and we will discuss how to take account of these selection effects in Buote et al. (2006a).

## 3. DATA REDUCTION

For data reduction, we used the *CIAO* 3.2.2 and *Heasoft* 5.3 software suites, in conjunction with *Chandra* calibration database (*Caldb*) version 3.1.0. Spectral-fitting was conducted with *Xspec* 11.3.1w. In order to ensure the most up-to-date calibration, all data were reprocessed from the "level 1" events files, following the standard *Chandra* data-reduction threads[5]. We applied the standard correction to take account of the time-dependent gain-drift as implemented in the standard *CIAO* tools. To identify periods of enhanced background ("flaring"), which seriously degrades the signal-to-noise (S/N) and complicates background subtraction (Markevitch 2002) we accumulated background lightcurves for each exposure from low surface-brightness regions of the active chips. We excluded obvious diffuse emission and data in the vicinity of any detected point-sources (see below). Periods of flaring were identified by eye and excised. Small amounts of residual flaring not removed by this procedure can be important in low surface-brightness regions at large radii, but this was taken into account in our treatment of the background (§ 3.1). The final exposure times are listed in Table 1.

Point source detection was performed using the *CIAO* tool `wavdetect` (Freeman et al. 2002). Point sources were identified in full-resolution images of the *ACIS* focal-plane, containing all active chips (except the S4 chip, which suffers from serious "streaking", which can lead to false detections). To maximise the likelihood of identifying sources with peculiarly hard or soft spectra, images were created in three energy bands, 0.1–10.0 keV, 0.1–3.0 keV and 3.0–10.0 keV. Sources were detected separately in each image. In order to minimize spurious detections at node or chip boundaries we supplied the detection algorithm with exposure-maps generated at energies 1.7 keV, 1.0 keV and 7 keV respectively (although the precise energies chosen made little difference to the results). The detection algorithm searched for structure over pixel-scales of 1, 2, 4, 8 and 16 pixels, and the detection threshold was set to ensure $\sim$0.1 spurious detections per image. The source-lists obtained within each energy-band were combined and duplicated sources removed, and the final list was checked by visual inspection of the images. The data in the vicinity of any detected point source were removed so as not to contaminate the diffuse emission. As discussed in Humphrey & Buote (2004, see also Kim & Fabbiano 2004) a significant fraction of faint X-ray binary sources will not have been detected by this procedure, and so we include an additional component to account for it in our spectral fitting (§ 5).

For each galaxy, we extracted spectra in a number of concentric annuli, centred on the nominal X-ray centroid. We determined the centroid iteratively by placing a $0.5'$ radius aperture at the nominal galaxy position (obtained from *NED*) and computing the X-ray centroid within it. The aperture was moved to the newly-computed centroid, and the procedure repeated until the computed

[5] http://cxc.harvard.edu/ciao/threads/index.html

TABLE 1
THE GALAXY SAMPLE

| Galaxy | Type | $L_B$ ($10^{10}L_\odot$) | $L_K$ ($10^{11}L_\odot$) | Dist (Mpc) | Scale ($''$ kpc$^{-1}$) | $R_{eff}$ (kpc) | ObsID | Date (dd/mm/yy) | Exposure (ks) |
|---|---|---|---|---|---|---|---|---|---|
| NGC 720 | E5 | 3.1 | 1.7 | 25.7 | 8.1 | 3.1 | 492 | 12/10/00 | 17 |
| NGC 1407 | E0 | 6.4 | 3.1 | 26.8 | 7.8 | 4.4 | 791 | 16/08/00 | 38 |
| NGC 4125 | E6 pec Liner | 4.7 | 1.8 | 22.2 | 9.4 | 3.3 | 2071 | 09/09/01 | 63 |
| NGC 4261 | E2-3 Liner Sy3 | 4.4 | 2.2 | 29.3 | 7.1 | 3.4 | 834 | 06/05/00 | 34 |
| NGC 4472 | E2/S0(2) Sy2 | 7.5 | 3.2 | 15.1 | 14 | 4.0 | 321 | 12/06/00 | 34 |
| NGC 4649 | E2 | 5.1 | 2.5 | 15.6 | 13 | 3.2 | 785 | 20/04/00 | 21 |
| NGC 6482 | E Liner | 10.9 | 3.2 | 58.8 | 3.6 | 3.4 | 3218 | 20/05/02 | 18 |

NOTE. — The galaxies in the sample. Distances were obtained from Tonry et al. (2001), corrected for the the new Cepheid zero-point (Jensen et al. 2003), except for NGC 6482, for which we adopted the kinematical distance modulus from *LEDA*. $L_B$ was obtained from *LEDA*, corrected to our distance. $K_s$-band luminosities ($L_K$) and effective radii ($R_{eff}$) were obtained from *2MASS*. We assumed $M_{B\odot} = 5.48$ and $M_{K\odot} = 3.41$ (e.g. Maraston 1998). We also list the image scale (Scale), which is the number of arc seconds corresponding to 1 kpc. We list the observation ID (ObsID) and total exposure times, after having eliminated flaring intervals.

position converged. Typically the X-ray centroid agreed with that from *NED*. The widths of the annuli were chosen so as to contain approximately the same number of background-subtracted photons and ensure there were sufficient photons in each to perform useful spectral-fitting. The data in the vicinity of any detected point-sources were excluded, as were the data from the vicinity of chip gaps, where the instrumental response may be uncertain. We extracted products from all active chips, excluding the S4, since it suffers from considerable "streaking" noise. Appropriate count-weighted spectral response matrices were generated for each annulus using the standard *CIAO* tasks **mkwarf** and **mkacisrmf**.

### 3.1. *Background estimation*

One of the chief difficulties in performing spectral-fitting of diffuse emission is the proper treatment of the background. A set of standard blank-field "template" files are available for *Chandra* as part of the *Caldb*. We found, however, that the background template files are not sufficiently accurate to use in the very low surface brightness regions at large radii, which are crucial to determine interesting global mass constraints. The background comprises cosmic, instrumental and non X-ray (particle) components. The cosmic component is known to vary from field to field, while the non X-ray background exhibits long-term secular variability. To mitigate the latter effect, several authors have adopted the practice of renormalizing the background template to ensure good agreement with their data at high energies ($\gtrsim 10$ keV). Such a procedure, however, also renormalizes the (uncorrelated) cosmic X-ray background and instrumental line features, which can lead to serious over- or under-subtraction. Given these reservations we chose to use an alternative background estimation procedure.

Our method involved modelling the background, somewhat akin to the approach of Buote et al. (2004). All of the targets were centred on the *ACIS*-S3 chip, which is back-illuminated (BI). To obtain constraints on the background, we extracted spectra from a $\sim 2'$ region centred on the S1 chip, which is also BI, and from an annulus centred at the galaxy centroid and with an inner and outer radii typically $\sim 2.5'$ and $3.3'$. We excluded data from the vicinity of any point-sources found by the source detection algorithm. Although the diffuse emission from each galaxy typically had a very low surface-brightness on the S1 CCD, we found that using two regions in this way with different contributions of source emission enabled the background components to be most cleanly disentangled from the source. The *ACIS* focal plane also consists of front-illuminated (FI) chips, which have significantly different (and lower) background. To obtain an estimate of the background for these chips, we extracted spectra from the entirety of each chip, excluding detected sources and data towards the edge of the chips where the exposure-map may be uncertain.

In order to constrain the model, we fitted all spectra simultaneously, without background subtraction, using *Xspec*. Our model consisted of a single APEC plasma (to take account of the diffuse emission from the galaxy; the "source"), plus background components. These comprised a power law with $\Gamma = 1.41$ (to account for the hard X-ray background), two APEC models with solar abundances and kT= 0.2 and 0.07 keV (to account for the soft X-ray background) and, to model the instrumental and particle contributions, a broken power law model and two Gaussian lines with energies 1.7 and 2.1 keV and negligible intrinsic widths. We have found that this model can be used to parameterize adequately the template background spectra. In general, the instrumental contributions of the FI chips were very similar in shape. Therefore, the background components of all the FI chips were tied, assuming the normalization scaled with the spectral extraction area. For the BI chips, there was some evidence that the S1 chip background can be somewhat larger at energies $\gtrsim 5$ keV (although this is variable). In order to disentangle the source and background components, given the general lack of photons in these spectra, we tied the abundances and temperatures of the "source" APEC components between the extraction regions, but allowed the normalizations to be free. Where there was a significant improvement in the fit-statistic if this assumption was relaxed, we allowed the abundances or temperatures to fit freely. Notwithstanding, this assumption should not significantly affect our results. This model was able to fit all of the data well. In our subsequent spectral analysis, we did not background-subtract the data using the standard templates, but took into account the background by using appropriately scaled versions of the models fitted to each

CCD, which were added according to the overlap between the source region and the CCD. We found that the standard background templates fared much worse than these modelled background estimates when the data were from regions of low surface-brightness. We discuss the impact of the background treatment on our results in § 7.3.

## 4. X-RAY IMAGES

The X-ray image of each galaxy was examined to identify any obvious surface-brightness disturbances or asymmetries which would be indicative of clear deviations from hydrostatic equilibrium. We note that low-level X-ray asymmetries, such as the "fingers of emission" identified by Randall et al. (2004) in the adaptively-smoothed images of NGC 4649, probably do not merit concern[6], as, provided care is taken to avoid seriously disturbed emission regions, reliable mass profiles can be inferred even in mildly disturbed systems (Buote & Tsai 1995).

In Fig 1 we show the 0.1–10.0 keV *ACIS*-S3 images of each of the systems. These images were first processed to remove point-sources, using the *CIAO* tool *dmfilth*, which replaces photons in the vicinity of each point-source with a locally-estimated background. NGC 4261 contains an AGN which appears as a bright central X-ray source and there is evidence of a small, low surface-brightness jet (Zezas et al. 2005). We have also removed these sources from the image. The images were flat-fielded with the 1.7 keV monochromatic exposure-map (although this analysis is insensitive to the choice of energy), and then smoothed by convolution with a $5''$ gaussian, to make large-scale structure more apparent. Due to the low surface-brightness nature of the emission at large radii, it is difficult to appreciate X-ray emission outside ∼a few arc minutes in many of the images. However, detailed spectral analysis and azimuthally-averaged surface brightness analysis reveals substantial hot gas extending beyond the edge of the S3 chip in each system.

None of the objects show very obvious disturbances in their X-ray emission on the *ACIS*-S3 chip (such as those found in NGC 4636: Jones et al. 2002). Some low-amplitude features are evident such as the faint jet in NGC 4261 (which is not visible in the above images), a possible north-south asymmetry in NGC 1407 and some asymmetry, in particular an off-axis X-ray enhancement, in NGC 4125. Based on adaptively-smoothed *XMM* images, Croston et al. (2005) argued that the X-ray emission in NGC 4261 is anti-correlated with the galaxy radio lobes. By inspection of the *XMM* images, this actually appears to be a very low-amplitude effect. It is not obvious in the *Chandra* images, although the X-ray isophotes do align somewhat perpendicularly to the jet. In any case, this does not appear to have significantly disturbed hydrostatic equilibrium, since there is excellent agreement between our inferred mass profile and a model comprising stellar plus DM components (§ 6), which would be an extraordinary coincidence if hydrostatic equilibrium had been strongly disturbed. The limited field-of-view makes it difficult to assess asymmetries and disturbances on the other chips. NGC 4472 is known, however, to exhibit a disturbance outside $\sim 6'$ (Irwin & Sarazin 1996), but mass analysis inside this radius should be reliable. We assess the impact of all these features in § 7.4.

[6] Although the authors suggested these may arise from bulk convective flow, the spectra do not agree with simulations of such.

## 5. SPECTRAL ANALYSIS

Spectral-fitting was carried out in the energy-band 0.5–7.0 keV, to avoid calibration uncertainties at lower energies and to minimize the instrumental background, which dominates at high energies. The spectra were rebinned to ensure a S/N ratio of at least 3 and a minimum of 20 photons per bin (to validate $\chi^2$ fitting). We fitted data from all annuli simultaneously using *Xspec*. To model the hot gas we adopted a **vapec** component, plus a bremsstrahlung component for all annuli within the twenty-fifth magnitude isophote ($D_{25}$) of each galaxy, taken from the Third Reference Catalog of Bright Galaxies (RC3: de Vaucouleurs et al. 1991), to account for undetected point-sources (this model gives a good fit to the composite spectrum of the detected sources in nearby galaxies: Irwin et al. 2003). We used a slightly modified form of the existing *Xspec* **vapec** implementation so that $Z_{Fe}$ is determined directly, but for the remaining elements the abundance ratios (in solar units) were directly determined with respect to Fe. This was useful since, in general, the data did not enable us to determine any abundance *ratio* gradients and so we tied the abundance ratios between all annuli. Where abundances or abundance ratios could not be constrained, they were fixed at the Solar value. We adopted the solar photospheric abundances standard of Asplund et al. (2004). We refer the interested reader to Humphrey & Buote (2006) for a detailed discussion of this choice and how to convert our results to older abundance standards. In the interests of physically reasonable results, we constrained all abundances and abundance ratios to the range 0.0–5.0 times solar. The absorbing column density ($N_{\rm H}$) was fixed at the Galactic value (Dickey & Lockman 1990); the effect of varying $N_{\rm H}$ is discussed in § 7.6. For NGC 4261, our innermost annulus contained substantial contamination from the central AGN. However, this was sufficiently absorbed that the thermal emission from the gas can be clearly disentangled from it. To account for the AGN emission, we fitted a highly absorbed ($N_{\rm H}= 10^{+6}_{-4} \times 10^{22}{\rm cm}^{-2}$) power law component ($\Gamma = 1.4 \pm 0.8$). We discuss the impact of including this annulus on our fits in § 7.4.

To account for projection effects, we used the **projct** model implemented in *Xspec*. This model, unfortunately, does not take into account the emission from gas outside the outermost shell, which is also projected into the line-of-sight. To take account of this effect, we assumed that the emission outside this shell has the same spectral shape as the emission in that shell and a density profile well-described by a $\beta$-model (e.g. Buote 2000). We included an extra spectral component to our fits of each annulus to account for projected emission from this gas. To estimate the parameters of the $\beta$-profile, we we fitted the galaxy surface brightness, using dedicated software, in the 0.1–3.0 keV band. Although a single $\beta$-model did not always match the fine detail of the surface brightness profiles, it adequately parameterized the data for our purposes (our results are not expected to be strongly dependent upon the parameters of this fit).

We obtained good fits to the spectra of each galaxy with this model. The best-fitting abundances were in excellent agreement with those of other early-type galaxies (Humphrey & Buote 2006), and are shown in Table 2.

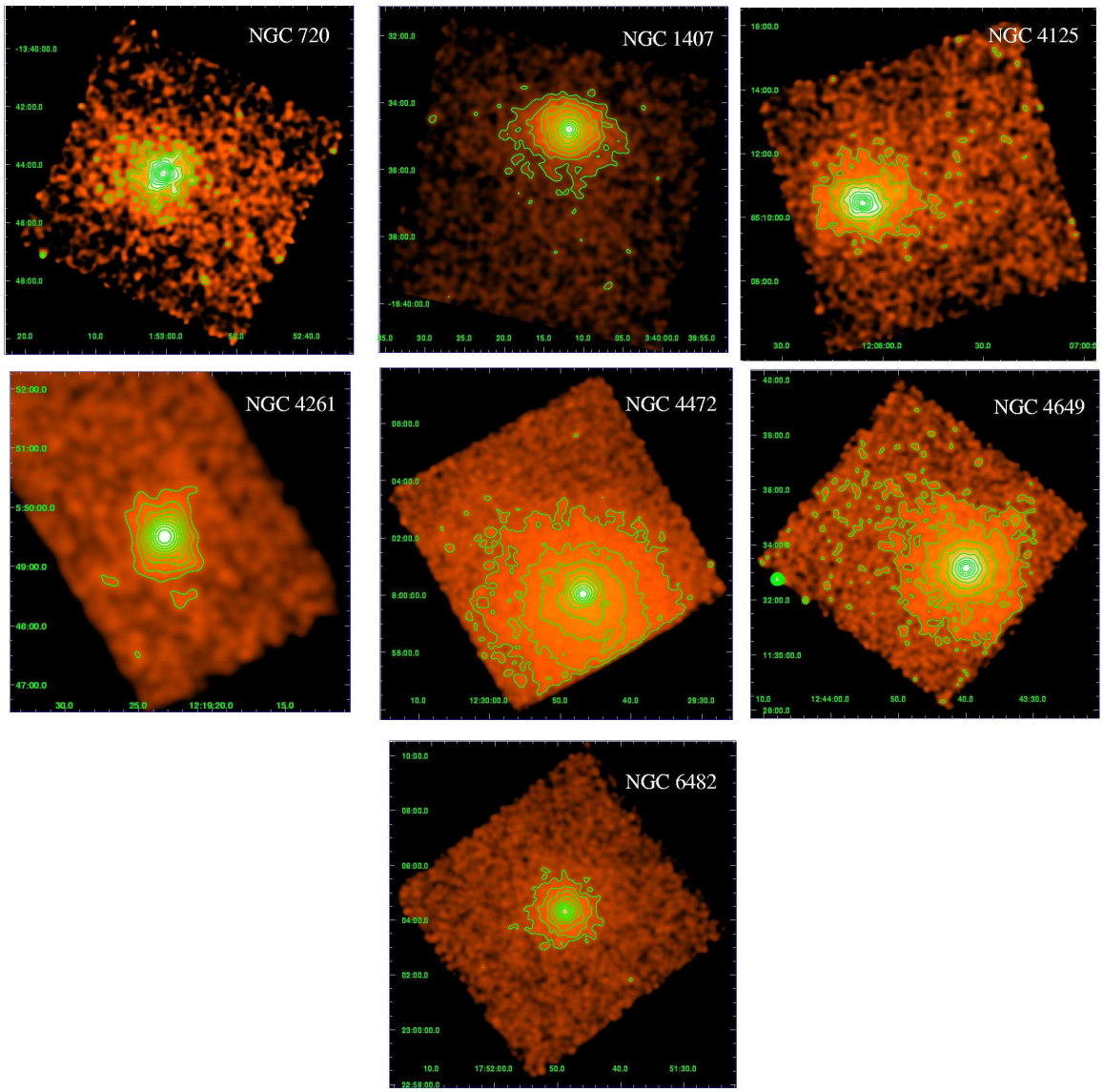


FIG. 1.— X-ray images of each of the galaxies in the sample. None of the systems show evidence of large-amplitude disturbances which would indicate a violation of hydrostatic equilibrium. Some lower-amplitude asymmetries do persist in some of the images, which we discuss in detail in § 7.4.

We note that Randall et al. (2006) found $Z_{Si}/Z_{Fe}\simeq1.7$ for NGC 4649 (adjusting to our abundances standard) when fitting the data from single, large aperture, which they argued points to substantial enrichment from SN II, in stark contrast to the predominantly SN Ia enrichment we found in such galaxies (Humphrey & Buote 2006). From our analysis, however, $Z_{Si}/Z_{Fe}\simeq1$, which is more consistent with our results for other systems. The discrepancy appears to be related to the "Fe bias" (where $Z_{Fe}$ is systematically underestimated if one assumes multi-temperature gas is isothermal: Buote 2000) which has suppressed their large aperture $Z_{Fe}$ in comparison to their spatially-resolved results (which agree better with our measurement).

Error-bars were computed *via* the Monte-Carlo technique which we have extensively used in past analyses (e.g. Buote et al. 2003). We simulated spectra from the best-fit models, which were then fitted exactly analogously to the real data. We performed 25 simulations, which were sufficient to assess the distribution of the fit parameters about the best-fit values; the standard deviation of this distribution corresponds to the 1-$\sigma$ confidence region.Assuming that we have found the global minimum, and the fit statistic follows a $\chi^2$ distribution this is statistically equivalent to searching the parameter space for changes in the fit statistic. Temperature and density profiles are discussed below (§ 6.2 and § 6.3)

## 6. MASS MODELLING

### 6.1. *Assumed potential method*

We adopted two complementary approaches in order to determine the mass profiles of the galaxies in the sample. The first method, discussed here, was found to be less sensitive to the assumptions of the modelling and therefore was adopted as our default. We discuss our alternative approach in § 6.4.

Starting with a parameterised model for the temperature (T) and gravitating mass ($M_{grav}$) profiles, the equa-

TABLE 2
EMISSION-WEIGHTED AVERAGE ABUNDANCES

| Galaxy | $\chi^2$/dof | $Z_{Fe}$ | $Z_O/Z_{Fe}$ | $Z_{Ne}/Z_{Fe}$ | $Z_{Mg}/Z_{Fe}$ | $Z_{Si}/Z_{Fe}$ | $Z_S/Z_{Fe}$ | $Z_{Ni}/Z_{Fe}$ |
|---|---|---|---|---|---|---|---|---|
| NGC 720[1] | 383.4/357 | $0.80^{+0.45}_{-0.24}$ | 0.30±0.28 | 0.68±0.67 | 1.26±0.35 | ... | ... | ... |
| NGC 1407[1] | 222/221 | $2.1^{+1.1\dagger}_{-0.9}$ | $0.37^{+0.21}_{-0.25}$ | ... | 1.10±0.23 | $1.21^{+0.31}_{-0.27}$ | 2.2±1.1 | $3.3^{+1.7}_{-1.3}$ |
| NGC 4125 | 327/307 | $0.55^{+0.22}_{-0.13}$ | $0.29^{+0.13}_{-0.09}$ | 0.62±0.14 | 0.33±0.20 | ... | ... | ... |
| NGC 4261 | 307/319 | 1.72±0.50† | <0.23 | $0.36^{+0.79}_{-0.36}$ | 0.83±0.23 | 1.2±0.4 | ... | $1.8^{+2.3}_{-1.8}$ |
| NGC 4649 | 563/491 | $2.32^{+0.87}_{-0.37}$ | < 0.15 | ... | 0.97±0.13 | 1.02±0.13 | ... | $1.42^{+0.85}_{-0.73}$ |
| NGC 4472[1] | 785/740 | $1.4^{+1.7\dagger}_{-0.4}$ | 0.51±0.12 | 0.95 ±0.44 | 1.02±0.11 | 1.25±0.11 | 2.36±0.33 | 3.28±0.61 |
| NGC 6482 | 256/262 | >2.5 | 0.34±0.20 | ... | 1.15±0.18 | 1.3±0.3 | ... | $3.2^{+1.5}_{-1.2}$ |

NOTE. — The best-fitting globally-averaged emission-weighted abundances and abundance ratios for each galaxy, shown along with the quality of fit. Statistical errors represent the 90% confidence region. Where we were able to constrain an abundance gradient, we estimated an emission-weighted $Z_{Fe}$, extrapolated over a large aperture (see Humphrey & Buote 2006); those affected galaxies are marked (†). [1]—results taken from Humphrey & Buote (2006). Where parameters could not be constrained, they were fixed at the Solar value, and listed as "...".

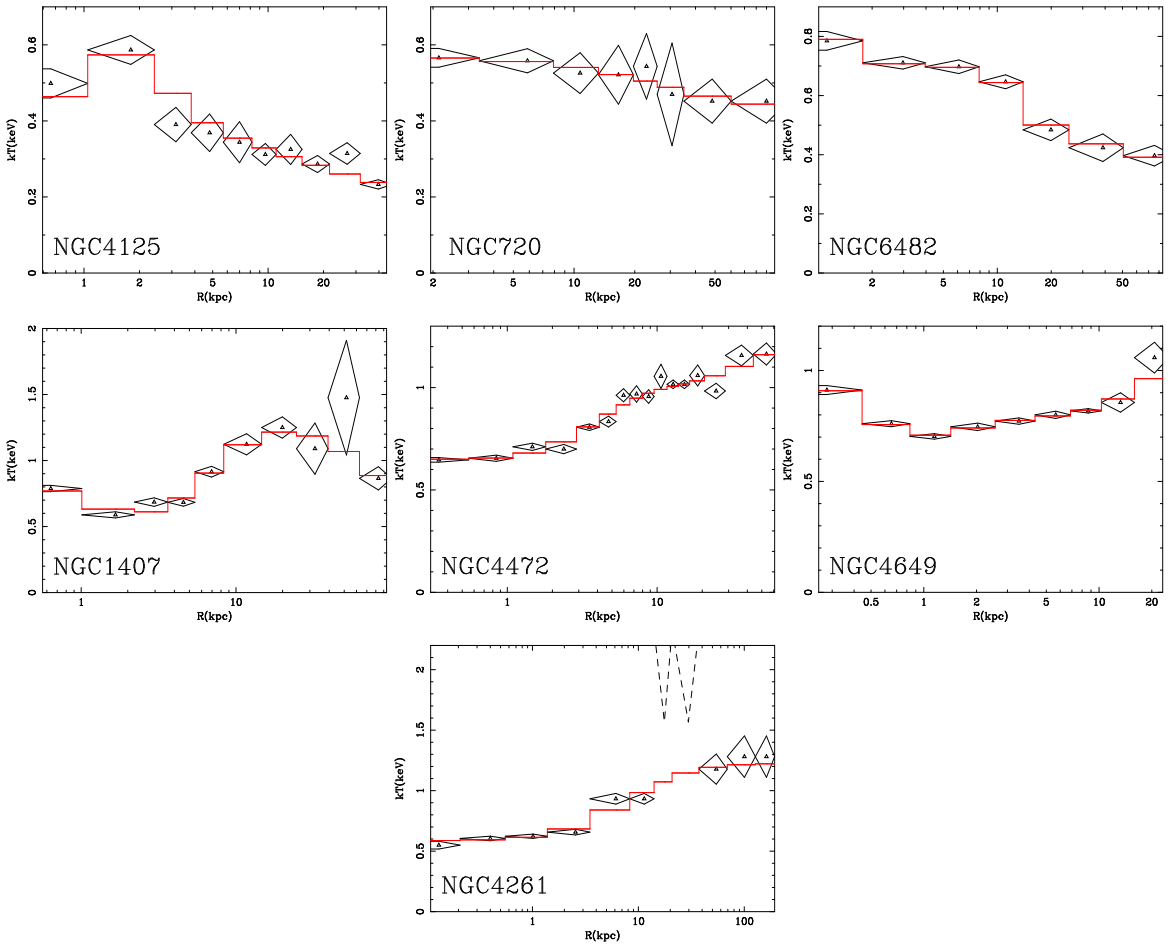


FIG. 2.— Deprojected temperature profiles of each galaxy, ordered by $M_{vir}$ (Table 6). The data-points are shown, along with the best-fit parameterized model determined from simultaneously fitting the $\rho_g$ and temperature profiles (see text). Where data-points were excluded from the fitting, they are denoted by dashed lines. Errors shown are 1-$\sigma$.

tion of hydrostatic equilibrium can be solved for $\rho_g$ thus:

$$\ln\left(\frac{\rho_g}{\rho_{g0}}\right) = -\ln\left(\frac{T}{T_0}\right) - G\mu m_p \int_{R_0}^{R} \frac{M_{grav}(<R)}{kTR^2} dR \quad (1)$$

where R is the radius from the centre of the gravitational potential, $\rho_g$ is the gas density, $\rho_{g0}$ and $T_0$ are density and temperature at some "reference" radius $R_0$, k is Boltzmann's constant, G is the universal gravitational constant, $m_p$ is the atomic mass unit and $\mu$ is the mean atomic weight of the gas. In our fitting we explicitly ignored the contribution of the gas to the gravitating mass, but we subsequently verified this contributed $\lesssim$1% of the total gravitating matter within 100 kpc, justifying this assumption. We developed software to fit $\rho_g$ and temperature profiles simultaneously using this proce-

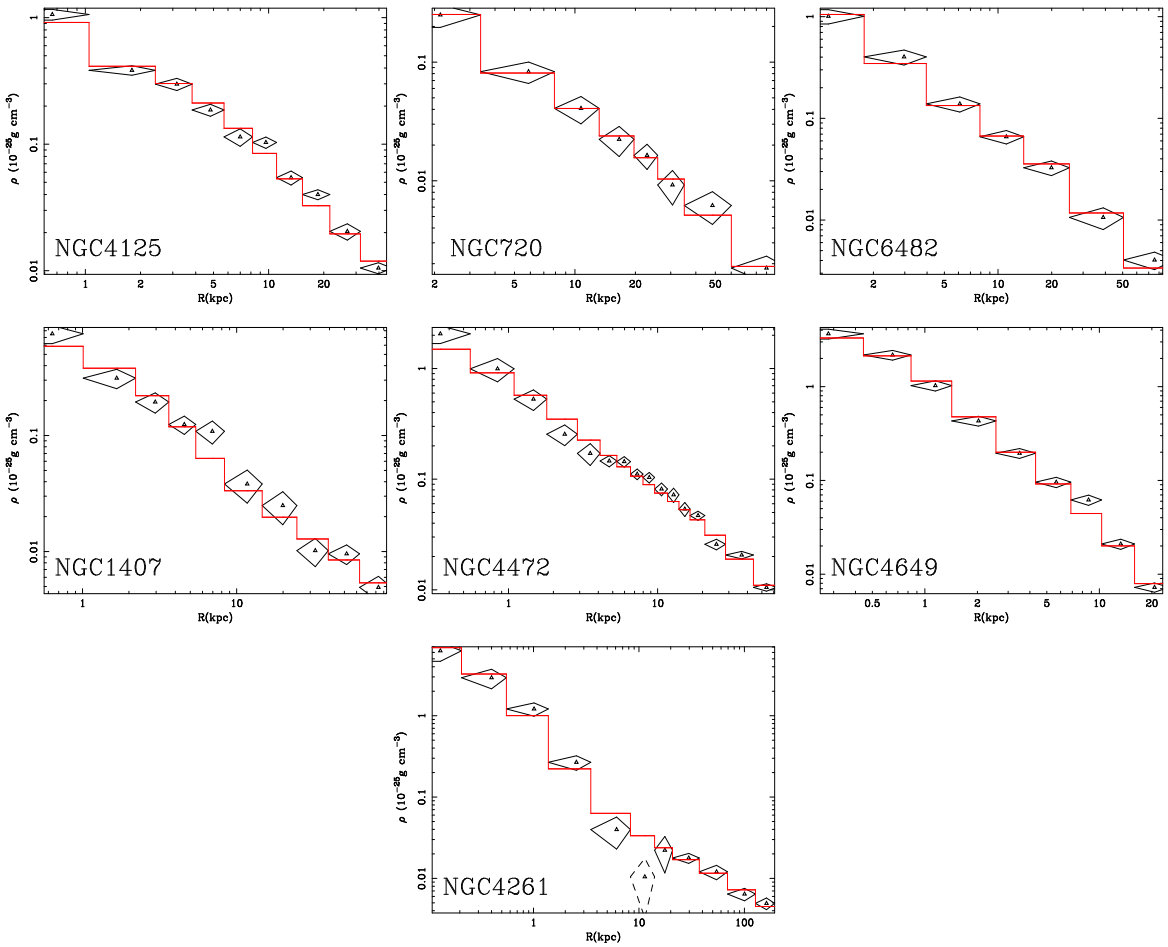


FIG. 3.— Deprojected density-profiles of each galaxy, shown with the best-fit AC NFW+stars model from the "assumed potential" modelling (§ 6.1). Data-points excluded from the fit are indicated by dashed lines. Errors shown are 1-$\sigma$.

dure. For speed we assumed that the density and temperature data-points were each evaluated at a single point, the radius of which was given by:

$$\bar{R}_i = \left(0.5 * (Rin_i^{1.5} + Rout_i^{1.5})\right)^{2/3} \quad (2)$$

where $Rin_i$ and $Rout_i$ were the inner and outer radius of the bin (see Lewis et al. 2003).

### 6.2. *Temperature profiles*

There were considerable differences in the temperature profiles from object to object (Fig 2), so that we were not able to adopt a "universal" profile for all of the systems. *A priori* we do not expect any particular form for the temperature profile and so we determined appropriate functional forms for our temperature models empirically. Based on experience, the following "toolbox" of models provided adequate flexibility to ensure at least one model can describe the temperature profiles reasonably well (see Buote et al. 2006b):

$$T = T_0 + T_1 \left[1 + x^{-\epsilon}\right]^{-1} \quad (3)$$

$$T = \left[T_0 + T_1 x^{p_1}\right] e^{-x^{p_e}} + T_2 x^{p_2} \left[1 - e^{-x^{p_e}}\right] \quad (4)$$

$$T = \frac{A}{A+B}\left[T_0 + T_1\left(\frac{x_1}{1+x_1}\right)^{p_1}\right] + \frac{B}{A+B}\left[T_2 + T_3(1+x_2)^{-p_2}\right] \quad (5)$$

where $x = (r/r_c)$, $x_1 = (r/r_{c1})$, $x_2 = (r/r_{c2})$, $A = (1 + r/r_{t1})^{-3\beta_1}$ and $B = \epsilon(1 + r/r_{t2})^{-3\beta_2}$. $T_0$, $T_1$, $T_2$, $T_3$, $r_c$, $r_{c1}$, $r_{c2}$, $r_{t1}$, $r_{t2}$, $p_1$, $p_2$, $p_e$ and $\epsilon$ are parameters of the fit. For NGC 4261, we ignored temperature data-points from 15–25 kpc, which were poorly-determined and seemed erroneous. We experimented with fitting the projected (rather than deprojected) spectra, and found no evidence of any features (in either temperature or density) around this range of radii, strongly implying that they arise solely due to deprojection noise. The temperature profiles and best-fit models are shown in Fig 2.

Our deprojected temperature profiles generally agree with those appearing in the literature for these objects. (Although most of these are projected profiles, typically deprojection does not strongly alter the overall character of the temperature profile.) O'Sullivan et al. (2003) reported *ROSAT* profiles for all of the galaxies which, although substantially less well-constrained, agree well with our results. Likewise our NGC 4472 temperature profile agrees well with the (less well-constrained) *ROSAT* profile of Irwin & Sarazin (1996). Our profile for NGC 4649 is in reasonable agreement with the projected *XMM* measurements of Randall et al. (2006), and likewise our measured profile of NGC 6482 agrees with the deprojected results of Khosroshahi et al. (2004). Our temperature profiles for NGC 1407, NGC 720 and

NGC 4472 were also in agreement with those we reported in Humphrey & Buote (2006).

### 6.3. *Mass-fitting results*

We tested three different mass-models against the data. In order to investigate the suggestion that historically large c values found based on X-ray analysis were an artefact of the omission of the stellar mass, as well as to investigate the scenario of Loeb & Peebles (2003), we first tested a model comprising a single NFW profile. Although stellar kinematical results would seem to rule out the Loeb & Peebles picture, our analysis of more massive systems (Gastaldello et al. 2006) does suggest that the stellar mass may not be uniformly required in all systems. In order to take into account the stellar mass, we fitted a model comprising an NFW DM component, plus a Hernquist (1990, hereafter H90) mass component, the $R_{\rm eff}$ of which being fixed to that measured in the $K_s$-band (Table 1). The H90 model is, in projection, a good approximation to the familiar de Vaucouleurs profile of elliptical galaxies. To test whether the DM halos retained any evidence of their response to baryonic condensation, we further adopted an H90 component, plus an NFW component modified by the adiabatic contraction model of Gnedin et al. (2004)[7]. Hereafter, we refer to these three models as, respectively, NFW, NFW+stars and AC NFW+stars. Our computed $M_{\rm vir}$ for each system included both dark and stellar mass. For NGC 4472 and NGC 4649, which lie in Virgo, there is the possibility that the DM halo may have experienced some tidal truncation at a radius $<R_{\rm vir}$. Our measured Virial quantities relate to the original halo prior to truncation. We also experimented with replacing the NFW component with the less cuspy Navarro et al. (2004, hereafter N04) model, which gives an improved fit to DM halos in high-resolution N-body simulations. However, since the $M_{\rm vir}$-c relation was calibrated using the NFW model we treat this choice as a systematic effect and it is discussed in § 7.1. For NGC 4261 we ignored a deviant $\rho_{\rm g}$ data-point at ∼11 kpc, in addition to the excluded temperature data-points discussed above.

In Fig 3 we show the density profiles (along with the best-fitting AC NFW+stars model, which is described below). In Fig 4(a) we show the best-fitting 1-$\sigma$ contours of c *versus* $M_{\rm vir}$ for the NFW model fitted to each galaxy. The fits were typically, but not uniformly, poor (Table 3). We found very large ($\gg$20) values for c, completely inconsistent with the expectation of N-body simulations.

Good constraints on the global halo properties typically require interesting density and temperature constraints over as large a radial range as possible. In our case, the absence of data outside ∼50–100 kpc (∼0.1–$0.2R_{\rm vir}$) therefore makes the inner data-points critical in determining the profile of the halo. Unfortunately, since the scale radius of a galaxy-size DM halo is ∼10–30 kpc, there is some degeneracy between the DM and stellar mass components at small radii. As we discuss in § 6.5 there are considerable uncertainties in estimating a reliable mass-to-light (M/L) ratio from the characteristics of the stellar population. We found that the results are extremely sensitive to the stellar M/L adopted; we found that varying this ratio by as little as 20% could cause $M_{\rm vir}$ variations of ∼50–100% (see Humphrey et al. 2005). It was therefore necessary to allow the stellar mass to be determined as a parameter of the fit. This, unfortunately, made it very difficult to constrain $M_{\rm vir}$ or c, unless additional constraints were applied to the fit.

One way to achieve this is to constrain the fit to lie on the mean $M_{\rm vir}$-c relation predicted from N-body simulations (e.g. Bullock et al. 2001). Although this would prevent our measuring $M_{\rm vir}$ and c independently, it would enable us to determine whether the data are consistent with the mean relation. However, this relation was determined for an unbiased sample of DM halos, whereas our selection criteria (§ 2) should bias us towards systems which have not recently had a merger (implying earlier-forming, hence more concentrated, objects). Furthermore, individual halos are not expected to lie exactly on the mean $M_{\rm vir}$-c relation, but be scattered about it. Nevertheless, we experimented with applying this constraint. The data for each galaxy were consistent with this model, but we found $M_{\rm vir}$ was generally poorly constrained, and extremely sensitive to any scatter we introduced about the mean $M_{\rm vir}$-c relation.

A far more useful way to constrain the fit was to restrict the total baryon fraction ($f_b$) in the system. Such a constraint is useful since we found that, for a given system, $f_b$ determined from our fits was strongly anti-correlated with the measured $M_{\rm vir}$. To estimate $f_b$, we computed the gas mass by extrapolating our $\rho_{\rm g}$ model from the centre of the innermost radial bin to the Virial radius. The contribution of stars to the total baryon fraction was derived from the stellar mass found by our fits. We crudely took into account the fact that not all of the stellar mass within $R_{\rm vir}$ is necessarily contained in the central galaxy by scaling this mass by the ratio of the total B-band light of all putative "group" members listed in the catalogue of Garcia (1993, hereafter G93) to that of the central galaxy. This is likely to overestimate slightly the stellar mass content, since it assumes the same stellar M/L ratio for all low-mass companions/ group members, whereas some fraction of these are likely to have substantial young stellar populations, with lower M/L ratios. We discuss the impact of this assumption in § 7.8. G93 lists NGC 4649 as belonging to the NGC 4472 "group", whereas they both have distinct X-ray halos, indicating they are, in fact, distinct systems. As a zeroth order approximation, we therefore assumed that the total B-band luminosity was divided between the two "subgroups" in proportion to the central galaxy's B-band luminosity. In practice, between ∼25% (for NGC 4472) and 84% (for NGC 4125) of the B-band light of the system resides in the central galaxy. NGC 6482 was not listed in G93, but as it is known to be relatively isolated (Khosroshahi et al. 2004), we assumed that ∼80% of its mass is in the central galaxy, consistent with the other relatively isolated systems.

Based on hydrodynamical simulations incorporating gas cooling and supernovae feedback, Kay et al. (2003) predicted $f_b$ as a function of Virial temperature for systems with $M_{\rm vir} \gtrsim$ a few $\times 10^{12} M_\odot$. Fitting their data by eye, converting from Virial temperature to mass, and assuming a Universal baryon fraction of 0.16, we estimate

$$f_b = 0.062 \log_{10}(M_{14}) + 0.13 \, (M_{14} < 1.02) \qquad (6)$$

[7] Available publicly from http://www.astronomy.ohio-state.edu/∼ognedin/contra/

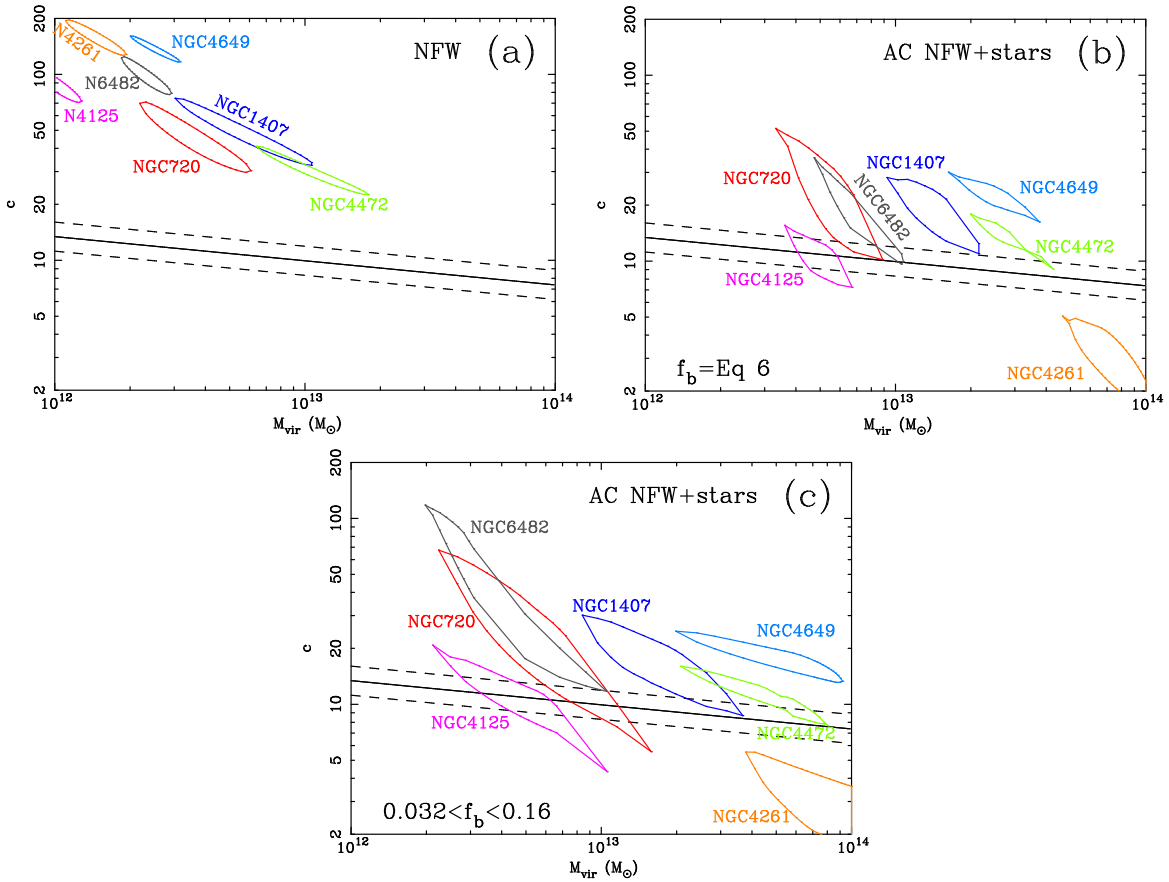


FIG. 4.— 1-$\sigma$ ($M_{vir}$,c) confidence regions for each object. Panel (a) shows the confidence contours found when fitting the NFW model. In panel (b) we show the contours for the AC NFW+stars model, restricting $f_b$ by Eq 6 (see text), and panel (c) shows contours for the same model, but now restricting $0.032 \leq f_b \leq 0.16$. The results for the NFW+stars model were very similar to those for the AC NFW+stars model. On each plot, we also show the prediction from the "toy model" of Bullock et al. (2001) (solid line) and the approximate 1-$\sigma$ scatter in the simulated DM halos (the region bounded by the dotted lines).

TABLE 3
QUALITY OF THE MASS FITS

| Galaxy | NFW | NFW+stars | AC NFW+stars |
|---|---|---|---|
| NGC 720 | 1.9/9 | 1.0/8 | 0.9/8 |
| NGC 1407 | 26.7/9 | 20.7/8 | 20.7/8 |
| NGC 4125 | 23.4/11 | 9.5/10 | 10.8/10 |
| NGC 4261 | 22.6/12 | 14.0/11 | 14.0/11 |
| NGC 4472 | 35.2/20 | 34.9/20 | 35.2/20 |
| NGC 4649 | 30.2/7 | 11.0/6 | 11.5/6 |
| NGC 6482 | 0.5/5 | 2.4/4 | 1.7/4 |

NOTE. — The $\chi^2$/dof of the fits to the density and temperature profiles used to infer the mass, for the three basic mass-models adopted. For the NFW+stars and AC NFW+stars models, we constrain $f_b$ to Eq 6.

$$f_b = \quad 0.14 \quad (M_{14} > 1.02)$$

where $M_{14} = M_{vir}/10^{14} M_\odot$, with an approximate scatter of $\pm 0.02$. Adopting this constraint (including the allowed range of scatter) and fitting the NFW+stars model resulted in significant improvements in the fit quality over the simple NFW model (Table 3). We show the resulting c-*versus*-$M_{vir}$ contours in Fig 4(b), and summarise our results in Table 4. Clearly adding the stellar mass component allows the DM halos to be substantially less concentrated, since less DM is required in the centre of the halo. These results were in much better agreement with the results of N-body simulations than those obtained with the NFW model. There is, however, a slight trend towards more concentrated halos than ΛCDM.

Since the results of simulations can be sensitive to the rather uncertain process of feedback, we additionally adopted, as a somewhat less restrictive constraint on $f_b$, $0.03 < f_b < 0.16$, the lower limit being ∼the lowest values found in Kay et al.'s simulations. The shallower potential of very low-mass halos makes it more difficult for them to hold onto their hot gas, and so our lower limit on $f_b$ may be an overestimate if the Virial mass is

TABLE 4
BEST-FITTING NFW+STARS RESULTS

| Galaxy | $f_b$=Eq 6 | | | | $0.032 \leq f_b \leq 0.16$ | | | |
|---|---|---|---|---|---|---|---|---|
| | $M_{vir}(10^{12}M_\odot)$ | $R_{vir}$(kpc) | c | $f_b$ | $M_{vir}(10^{12}M_\odot)$ | $R_{vir}$(kpc) | c | $f_b$ |
| NGC720 | $6.6^{+2.4}_{-3.0}$ | $480^{+50}_{-90}$ | $18.^{+30.}_{-8.}$ | $0.044^{+0.037}_{-0.003}$ | $6.6^{+6.0}_{-4.3}$ | $480 \pm 120$ | $18.^{+49.}_{-10.}$ | $0.044^{+0.095}_{-0.012}$ |
| NGC1407 | $16. \pm 6.$ | $650^{+80}_{-100}$ | $18.^{+11.}_{-7.}$ | $0.065^{+0.041}_{-0.001}$ | $21. \pm 15.$ | $720^{+140}_{-200}$ | $15.^{+16.}_{-6.}$ | $0.032^{+0.130}_{-0.001}$ |
| NGC4125 | $6.2^{+0.8}_{-2.3}$ | $470^{+20}_{-70}$ | $10.^{+5.}_{-2.}$ | $0.039^{+0.035}_{-0.001}$ | $7.2^{+1.4}_{-4.9}$ | $500^{+30}_{-160}$ | $9.3^{+11.}_{-2.1}$ | $0.032^{+0.13}_{-0.001}$ |
| NGC4261 | $67.^{+41.}_{-15.}$ | $1040^{+200}_{-90}$ | $3.7 \pm 1.7$ | $0.14^{+0.01}_{-0.03}$ | $57.^{+260}_{-15.}$ | $990^{+760}_{-100}$ | $4.0 \pm 2.0$ | $0.16^{+0.00}_{-0.13}$ |
| NGC4472 | $33.^{+6.}_{-10.}$ | $820^{+50}_{-100}$ | $13.^{+4.}_{-2.}$ | $0.084^{+0.037}_{-0.001}$ | $63.^{+17.}_{-44.}$ | $1020^{+90}_{-300}$ | $10.0^{+7.}_{-2.}$ | $0.032^{+0.13}_{-0.00}$ |
| NGC4649 | $35.^{+7.}_{-13.}$ | $840^{+60}_{-120}$ | $21.^{+6.}_{-3.}$ | $0.086^{+0.037}_{-0.001}$ | $93.^{+26.}_{-73.}$ | $1200^{+100}_{-500}$ | $15.^{+11.}_{-3.}$ | $0.032^{+0.12}_{-0.00}$ |
| NGC6482 | $7.1^{+4.4}_{-1.7}$ | $500^{+90}_{-40}$ | $18.^{+13.}_{-8.}$ | $0.075^{+0.013}_{-0.032}$ | $3.6^{+5.5}_{-1.5}$ | $390^{+140}_{-70}$ | $38.^{+76.}_{-24.}$ | $0.16^{+0.00}_{-0.10}$ |

NOTE. — The best-fitting results for the NFW+stars model. All error-bars shown correspond to 90% confidence regions. The fit results for the AC NFW+stars model are very similar, and are shown in Fig 4. Results are shown for the fits using the two different constraints on $f_b$ we adopted (see text).

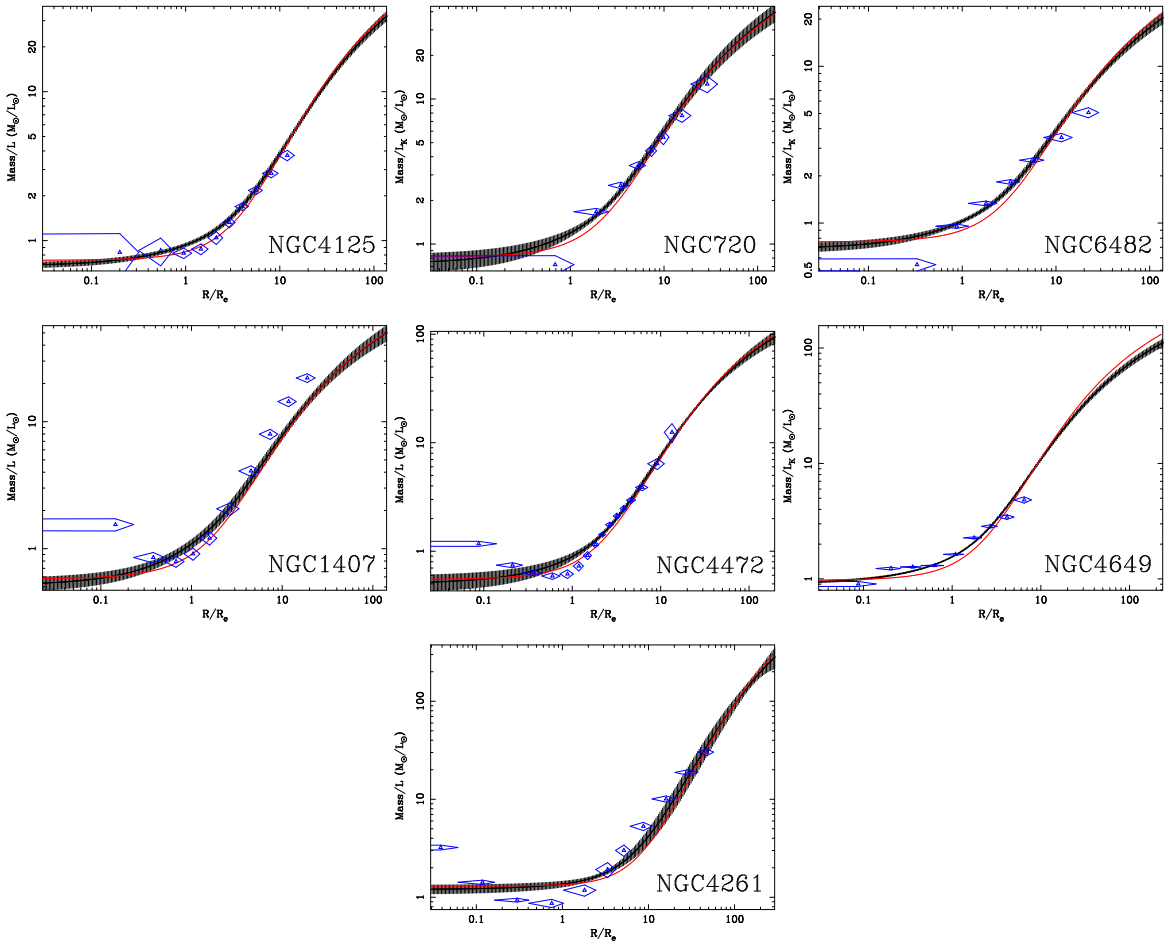


FIG. 5.— The K-band mass-to-light profile of each galaxy. Results are shown both for the NFW+stars and the AC NFW+stars models. For the latter the shaded region indicates the approximate 1-$\sigma$ confidence region. We also show data-points derived from the "parameterized profile" mass-modelling described in § 6.4. We stress that these data-points are *not* fitted by the models shown here, but they are derived independently.

small. However, imposing a lower limit on $f_b$ in the fitting algorithm actually works to exclude the most massive solutions, which we would expect to be closer to baryonic closure (Mathews et al. 2005). It is conceivable that some more massive ($M_{vir} \gtrsim 10^{13} M_\odot$) systems are rare examples of "dark" groups which have unusually low baryon fractions, a possibility we return to in § 8.7. Notwithstanding, the results are shown in Figs 4(c), which are qualitatively similar to those obtained applying the more restrictive constraint on $f_b$, although with larger uncertainty.

In Fig 5 we show the gravitating mass to K-band light ($M_{grav}/L_K$) ratio profile implied by our best-fit models for each system. In each case we found that the X-ray emission was considerably more extended than the optical light. We also show data-points estimated from "pa-

rameterized profile" mass modelling (§ 6.4), which tend to agree reasonably well; the slight systematic differences between the profiles are an artefact of the assumptions used to derive the data-points and we discuss this in detail in § 6.4. Clearly $M_{grav}/L_K$ increases very slowly with radius within $R_{eff}$, rising very steeply outside this range. This arises naturally from the very different shapes of the stellar and DM halos, and is similar to M/L profiles seen from stellar kinematics and the results of Brighenti & Mathews (1997) for NGC 4472 and NGC 4649. By $R_{vir}$, $M_{grav}/L_K$ reaches as high as $\sim$20–40 $M_\odot/L_\odot$ for the galaxy-scale systems or $\sim$100-200 $M_\odot/L_\odot$ for the group-like objects. We stress that this only includes the light of the central galaxy which, for the group-like systems may be a little as $\sim$25% of the total luminosity.

### 6.4. *Parameterized profile mass modelling*

We briefly discuss here an alternative technique to determine the mass profiles of X-ray bright objects which we have extensively employed in our previous studies, as well as the companion papers to this present work (e.g. Lewis et al. 2003; Buote et al. 2006b; Gastaldello et al. 2006; Zappacosta et al. 2006). This technique, which we here dub the "parameterized profile" method involves parameterizing independently the temperature and density profiles of the system with simple, empirical models. These functions were then inserted into the equation of hydrostatic equilibrium, which we solved for the mass enclosed within any given radius. The temperature profiles were parameterized with the models discussed in § 6.2, and to fit $\rho_g$ we adopted, where appropriate a, $\beta$-model, a "double-$\beta$" model or a "cusped-$\beta$" model, defined, respectively, as:

$$\rho_g = \rho_{g0}\left[1+(r/r_c)^2\right]^{-3\beta/2} \quad (7)$$

$$\rho_g = \sqrt{\rho_{g0}\left[1+(r/r_c)^2\right]^{-3\beta} + \rho_{g1}\left[1+(r/r_{c2})^2\right]^{-3\beta_2}} \quad (8)$$

$$\rho_g = \rho_{g0} 2^{3\beta/2-\epsilon/2}(r/r_c)^{-\epsilon}\left[1+(r/r_c)^2\right]^{-3\beta/2+\epsilon/2} \quad (9)$$

Where the parameters $\rho_{g0}$, $\rho_{g1}$, $r_c$, $r_{c2}$, $\beta$, $\beta_2$ and $\epsilon$ are determined by the fit. Fitting these models to the simulated temperature and density profiles discussed in § 5 (which were used therein to estimate the error-bars on kT and $\rho_g$ in each data-bin) allowed us to estimate the scatter in the mass data-points arising from statistical noise, and hence the error-bars.

For a full discussion of this technique, we refer the interested reader to Buote et al. (2006b), who demonstrate the good agreement typically found between this method and the assumed potential modelling of § 6.1, when fitting high-quality data. However, the mass data-points, especially at the innermost and outermost radii, are rather sensitive to the parameterized models adopted to fit the temperature and, especially, $\rho_g$. The systematic uncertainty introduced by the choice of $\rho_g$ model can be considerably larger than the statistical error. For our purposes the absence of data at very large radii, which are vital to constrain the curvature of the mass model, exacerbated by the uncertainty introduced at small radii due to the uncertain stellar mass-to-light ratio, magnified the impact of these systematic effects. Notwithstanding these reservations, it is still interesting to compare the results obtained *via* both mass-fitting methods. We show in Fig 6 the mass data-points computed using parameterized potential modelling, along with the best-fitting mass models found in § 6.1. Clearly there is good overall agreement between the two methods although there are some systematic differences, which reflect the systematics inherent in our choice of parameterized model for $\rho_g$.

### 6.5. *Stellar mass-to-Light ratios*

It is interesting to compare the stellar M/L ratios ($M_*/L$) determined by our fitting to the expectations of stellar population synthesis models. In order to ensure that the optical light traces the stellar mass as closely as possible, we opted to perform this comparison in the K-band. Table 5 shows $M_*/L_K$ determined from our models using eq 6 to constrain $f_b$. Since AC tends to increase the cuspiness of the DM profile we found a significantly lower mass-to-light ratio for the AC NFW+stars model than for the NFW+stars model.

To compare our measured $M_*/L_K$ to single burst stellar population synthesis predictions, we first estimated a mean emission-weighted stellar age and metallicity for each galaxy, as outlined in Appendix A. We linearly interpolated synthetic $M_*/L_K$ values based on the stellar population models of Maraston (1998) from updated model-grids made available by the author[8]. For typical early-type galaxies, K-band and *2MASS* $K_s$-band magnitudes should differ by <0.1 magnitudes (Carpenter 2001), so we were able to compare directly the synthetic K-band M/L ratios with our measured $M_*/L_K$ ratios. The predicted $M_*/L_K$ ratios are shown in Table 5 for different assumptions about the stellar IMF, which is poorly-known in early-type galaxies. In this case we show predicted $M_*/L_K$ assuming a standard Salpeter IMF, and for the IMF of Kroupa (2001). It is immediately clear that these ratios are very sensitive to this choice; $M_*/L_K$ is typically $\sim$50–60% higher if the Salpeter IMF is used.

Our measured $M_*/L_K$ for the NFW+stars models are typically $\sim$20% lower than the synthetic M/L ratios, assuming the Kroupa IMF. Using the AC NFW+stars models, the discrepancy is $\sim$40%. Assuming a Salpeter IMF, the discrepancies for both models are considerably larger. This would seem to rule out the Salpeter IMF, in agreement with the conclusions of Padmanabhan et al. (2004). The best-fitting $M_{vir}$ and c are sensitive to $M_*/L_K$. If we fix $M_*/L_K$ to the synthetic value, this essentially pushes all the galaxies, except NGC 4261 (for which the measured and synthetic values are in excellent agreement) and NGC 720 in the direction of the high-$M_{vir}$ range of their confidence contours shown in Fig 4. For NGC 720, $M_{vir}$ is lowered and c increased. The fits are then typically much worse ($\Delta\chi^2$ $\sim$7–35), and the loci in the $M_{vir}$-c plane slightly more discrepant with simulations.

There are a considerable number of systematic uncertainties in the computation of the synthetic M/L ratios, not the least of which is the very uncertain IMF, which could probably account for the modest discrepancy with our NFW+stars results (see § 8.4). In the case of NGC 720, the rather young age inferred for the stellar population ($\sim$3 Gyr) leads to a significantly lower

[8] http://www-astro.physics.ox.ac.uk/~maraston/Claudia's_Stellar_Population_Models.html

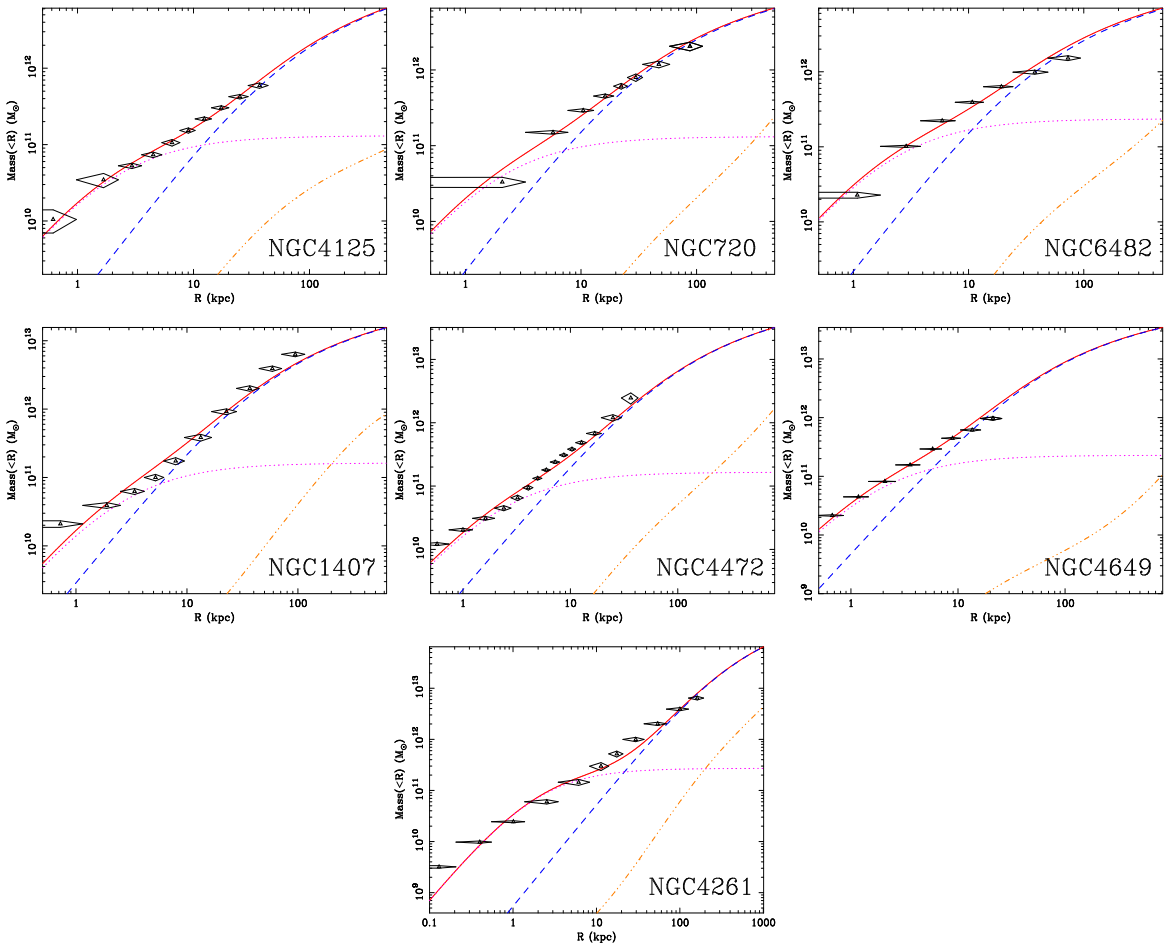


FIG. 6.— Mass profiles for each galaxy. The data-points were computed using parameterized profile modelling (§ 6.4). In addition we show the best-fit NFW+stars mass models from assumed potential modelling, which generally agree reasonably well with the data-points, indicating the consistency of both approaches to determine the mass profiles. We show the total gravitating mass model (solid line) and, separately, the stellar mass contribution (dotted line), the DM contribution (dashed line) and the gas mass (dash-dot-dot line). The models are extrapolated out to $R_{vir}$.Errors shown are 1-$\sigma$.

TABLE 5
STELLAR MASS-TO-LIGHT RATIOS

| Galaxy | $L_K/L_B$ | Fitted $M_*/L_K$ ($M_\odot/L_\odot$) | | Pop. synthesis $M_*/L_K$ ($M_\odot/L_\odot$) | |
|---|---|---|---|---|---|
| | | NFW+stars | AC NFW+stars | Salpeter IMF | Kroupa IMF |
| NGC 720 | 5.5 | $0.77^{+0.52}_{-0.71}$ | $0.54^{+0.42}_{-0.48}$ | 0.54±0.11 | 0.35±0.07 |
| NGC 1407 | 4.8 | $0.52^{+0.25}_{-0.32}$ | 0.35±0.25 | 1.6±0.2 | 1.1±0.1 |
| NGC 4125 | 3.8 | 0.72±0.11 | 0.53±0.11 | 1.7±0.5 | 1.1±0.4 |
| NGC 4261 | 5.0 | 1.2±0.1 | 1.0±0.1 | 1.9±0.1 | 1.3±0.1 |
| NGC 4472 | 4.3 | $0.51^{+0.24}_{-0.31}$ | 0.36±0.1 | 1.3±0.3 | 0.83±0.15 |
| NGC 4649 | 4.9 | 0.90±0.13 | 0.65±0.12 | 1.7±0.2 | 1.1±0.1 |
| NGC 6482 | 2.9 | $0.73^{+0.18}_{-0.27}$ | $0.52^{+0.19}_{-0.23}$ | 1.58±0.02 | 1.05±0.02 |

NOTE. — K-band stellar mass-to-light ratios measured from our fits to the data using both the NFW+stars and the AC NFW+stars models. Since AC tends to increase the cuspiness of the DM profiles, $M_*/L_K$ is substantially lower for the AC NFW+stars models. We also show the predicted $M_*/L_K$ values derived from simple stellar population synthesis, assuming either the Salpeter or Kroupa (2001) IMF.

synthetic $M_*/L_K$ than measured. Fitting template models to spatially-resolved spectra of this system, Rembold et al. (2005) found evidence of a significant age gradient, which falls from ∼12 Gyr in the centre to ∼3 Gyr by 1 kpc. This may, therefore, represent a system in which a relatively small fraction of the stellar component, produced in a modest, recent star-formation event ("frosting") dominates the optical line emission. In this case, the synthetic $M_*/L_K$ may be underestimated. We return to this issue in § 8.4.

## 7. SYSTEMATIC ERRORS

TABLE 6
Systematic error budget

| Galaxy | Best-fit | Δstat | ΔN04 | Δstars | Δbkd | Δasym | Δtemp | Δspectra | Δdist | Δbaryons |
|---|---|---|---|---|---|---|---|---|---|---|
| | | | | | $M_{vir}/10^{12}M_{\odot}$ | | | | | |
| NGC720 | 6.6 | $^{+2.4}_{-3.0}$ | +0.06 | $^{+0.5}_{-0.3}$ | −1.7 | −0.2 | −0.9 | $^{+0.7}_{-0.2}$ | $^{+0.9}_{-0.6}$ | −0.01 |
| NGC1407 | 16 | ±6 | −0.1 | $^{+1}_{-0.5}$ | −3 | +3 | $^{+1}_{-3}$ | $^{+1}_{-3}$ | $^{+3}_{-4}$ | −0.3 |
| NGC4125 | 6.2 | $^{+0.8}_{-2.3}$ | −0.2 | $^{+1.7}_{-2.1}$ | $^{+0.09}_{-0.2}$ | $^{+0.2}_{-0.03}$ | −1.0 | $^{+0.5}_{-2.0}$ | $^{+0.7}_{-0.6}$ | −0.3 |
| NGC4261 | 67 | $^{+41}_{-15}$ | +2 | $^{+15}_{-24}$ | +9 | $^{+5}_{-0.5}$ | $^{+0.08}_{-0.6}$ | $^{+13}_{-0.04}$ | $^{+4}_{-7}$ | −3 |
| NGC4472 | 33 | $^{+6}_{-10}$ | +0.5 | $^{+6}_{-0.05}$ | +2 | +12 | −4 | $^{+8}_{-1}$ | ±3 | −5 |
| NGC4649 | 35 | $^{+7}_{-13}$ | −8 | $^{+16}_{-3}$ | +2 | −1 | $^{+63}_{-2}$ | $^{+6}_{-2}$ | ±3 | −19 |
| NGC6482 | 7.1 | $^{+4.4}_{-1.7}$ | −0.8 | $^{+1.9}_{-0.3}$ | −0.1 | +0.8 | $^{+0.1}_{-3.6}$ | $^{+0.3}_{-0.8}$ | $^{+0.9}_{-0.8}$ | −0.2 |
| | | | | | c | | | | | |
| NGC720 | 18 | $^{+30}_{-8}$ | +0.1 | ±2 | +6 | +0.2 | +2 | $^{+2}_{-1}$ | ±2 | +0.03 |
| NGC1407 | 18 | $^{+11}_{-7}$ | −0.8 | $^{+2}_{-3}$ | $^{+4}_{-3}$ | −4 | $^{+4}_{-1}$ | $^{+6}_{-3}$ | $^{+5}_{-3}$ | +0.02 |
| NGC4125 | 10 | $^{+5}_{-2}$ | −1 | $^{+5}_{-4}$ | $^{+0.9}_{-0.1}$ | $^{+0.05}_{-1.0}$ | +2 | $^{+2.}_{-0.7}$ | $^{+2}_{-1}$ | +0.3 |
| NGC4261 | 3.7 | ±1.7 | −1.4 | $^{+3.6}_{-1.2}$ | $^{+0.10}_{-0.7}$ | −0.3 | $^{+0.08}_{-0.03}$ | −1.5 | $^{+0.8}_{-0.1}$ | +0.08 |
| NGC4472 | 13 | $^{+4}_{-2}$ | −2 | $^{+0.4}_{-2}$ | −0.7 | −5 | +1 | $^{+0.2}_{-3.}$ | ±2. | +1.0 |
| NGC4649 | 21 | $^{+6}_{-3}$ | −2 | $^{+3}_{-6}$ | −0.9 | +2 | $^{+3}_{-4}$ | $^{+0.4}_{-3}$ | ±3 | +7 |
| NGC6482 | 18 | $^{+13}_{-8}$ | +1 | $^{+2}_{-6}$ | +3 | +6 | $^{+51.}_{-0.4}$ | +2 | ±3 | −0.7 |
| | | | | | $M_*/L_K$(NFW+stars) | | | | | |
| NGC720 | 0.77 | $^{+0.52}_{-0.71}$ | +0.17 | $^{+0.28}_{-0.18}$ | −0.15 | +0.07 | −0.04 | ±0.10 | ±0.16 | −0.001 |
| NGC1407 | 0.52 | $^{+0.25}_{-0.32}$ | +0.06 | $^{+0.71}_{-0.16}$ | $^{+0.12}_{-0.04}$ | +0.14 | −0.19 | $^{+0.09}_{-0.18}$ | $^{+0.10}_{-0.08}$ | +0.001 |
| NGC4125 | 0.72 | ±0.11 | +0.04 | $^{+0.62}_{-0.20}$ | $^{+0.01}_{-0.03}$ | +0.06 | −0.04 | +0.05 | ±0.15 | −0.003 |
| NGC4261 | 1.2 | ±0.1 | +0.05 | $^{+0.7}_{-0.8}$ | $^{+0.008}_{-0.001}$ | $^{+0.04}_{-0.05}$ | $^{+0.0009}_{-0.006}$ | $^{+0.09}_{-0.010}$ | ±0.2 | −0.006 |
| NGC4472 | 0.51 | $^{+0.24}_{-0.31}$ | +0.06 | $^{+0.45}_{-0.06}$ | +0.05 | +0.20 | −0.01 | $^{+0.13}_{-0.02}$ | $^{+0.11}_{-0.09}$ | −0.01 |
| NGC4649 | 0.91 | ±0.13 | +47 | $^{+0.80}_{-0.19}$ | +0.02 | −0.06 | −0.16 | $^{+0.05}_{-0.009}$ | ±0.18 | −0.03 |
| NGC6482 | 0.73 | $^{+0.18}_{-0.27}$ | +0.13 | $^{+0.50}_{-0.04}$ | −0.06 | −0.15 | −0.51 | −0.05 | ±0.15 | −0.01 |
| | | | | | $M_*/L_K$(AC NFW+stars) | | | | | |
| NGC720 | 0.54 | $^{+0.42}_{-0.48}$ | −0.12 | ±0.16 | −0.14 | +0.06 | −0.05 | $^{+0.03}_{-0.10}$ | $^{+0.12}_{-0.09}$ | −0.003 |
| NGC1407 | 0.35 | ±0.25 | −0.06 | $^{+0.41}_{-0.08}$ | $^{+0.12}_{-0.05}$ | +0.12 | −0.14 | $^{+0.07}_{-0.13}$ | $^{+0.07}_{-0.05}$ | −0.001 |
| NGC4125 | 0.53 | ±0.11 | −0.04 | $^{+0.46}_{-0.14}$ | $^{+0.01}_{-0.03}$ | +0.06 | −0.04 | +0.04 | $^{+0.11}_{-0.09}$ | −0.002 |
| NGC4261 | 1.0 | ±0.1 | +0.02 | ±0.6 | $^{+0.02}_{-0.004}$ | $^{+0.03}_{-0.04}$ | −0.006 | $^{+0.1}_{-0.003}$ | ±0.2 | −0.009 |
| NGC4472 | 0.36 | ±0.1 | −0.04 | $^{+0.27}_{-0.03}$ | +0.04 | +0.17 | −0.02 | $^{+0.09}_{-0.01}$ | $^{+0.08}_{-0.06}$ | −0.010 |
| NGC4649 | 0.65 | ±0.12 | −0.05 | $^{+0.57}_{-0.12}$ | +0.02 | −0.06 | −0.13 | $^{+0.06}_{-0.008}$ | ±0.13 | −0.05 |
| NGC6482 | 0.52 | $^{+0.19}_{-0.23}$ | −0.07 | $^{+0.37}_{-0.03}$ | −0.05 | −0.13 | $^{+0.005}_{-0.03}$ | −0.04 | $^{+0.11}_{-0.09}$ | −0.01 |

Note. — The estimated error-budget for each of the galaxies. Excepting the statistical error, these values estimate a likely upper bound on the sensitivity of the (best fit) value of each parameter to various data-analysis choices, and should *not* be added in quadrature with the statistical errors. The systematic uncertainties on $M_{vir}$ and c are estimated for the NFW+stars model. In addition to the best-fit values, we show the 90% confidence interval for each parameter (Δstat). We also show estimated upper-limits on the systematics likely to arise by making various changes to our default analysis choices. This includes adopting the N04 DM model (ΔN04), varying the shape of the stellar mass component (Δstars), varying the background (Δbkd), excluding data in the vicinity of asymmetries (Δasym), adopting alternative temperature models (Δtemp), changing spectral analysis choices (Δspectra), varying the distance (Δdist) or assuming that all of the stellar baryons are in the central galaxy (Δbaryons).

In this section we address the sensitivity of our results to various data-analysis choices which were made. An estimated upper limit on the sensitivity of our results to these choices is shown in Table 6. These numbers reflect the sensitivity in the best-fit parameter to each potential source of systematic error, and we stress they should *not* be added in quadrature with the statistical errors. We outline in detail below how each of these systematics were estimated. Those readers uninterested in the technical details of our analysis may like to proceed directly to § 8.

### 7.1. *DM profile shape*

As discussed above, we experimented with replacing the NFW model by the revised N04 model, which is less cuspy. We caution that the $M_{vir}$-c relation was derived assuming NFW. We fixed the $\alpha$ parameter for this model to 0.17, the mean value determined from simulations since the inner slope of the DM halo is degenerate to some degree with the stellar mass. The quality of the fits (N04+stars, AC N04+stars) were typically similar to those using the simple NFW profile. There were some slight systematic differences in the inferred $M_{vir}$ and c as compared to NFW. It is interesting to note that this model, which is less cuspy than NFW, gave slightly larger $M_*/L_K$, although not sufficiently to bring our measurements completely into agreement with the synthetic estimates. For the adiabatically-compressed N04 model, $M_*/L_K$ did not increase, but this is unsurprising since the stellar component significantly modifies the shape of the inner DM halo in this model. We note that the predicted typical inner slope for ΛCDM halos is still under debate. If, instead of the N04 profile we had adopted the cuspier profile of Diemand et al. (2005), then the resul-

tant $M_*/L_K$would have been even smaller, and in worse agreement with stellar population models.

### 7.2. *Shape of the stellar potential*

To account for the stellar component, we adopted an H90 model, the effective radius of the model being fixed to that determined by *2MASS*. However, it is not entirely clear that the H90 model is an adequate description of the stellar mass. There are some deviations between H90 and the de Vaucouleurs model fitted as the *de facto* standard to the optical light profiles of elliptical galaxies, particularly in the critical central regions. Furthermore, the K-band light profiles of elliptical galaxies may, in fact, be better described by the Sérsic profile (e.g. Brown et al. 2003). To investigate the sensitivity of our results to the H90 assumption, therefore, we experimented with adopting a Sérsic stellar mass potential (e.g. Prugniel & Simien 1997). To determine the two parameters of this model (the Sérsic index and half-light radius) we obtained the $K_s$-band *2MASS* images of each galaxy from *NED*, and fitted the surface brightness profiles using dedicated software. A Sérsic model fitted the $K_s$-band light profile of each galaxy in the radial range $5''$–$3'$ reasonably well. The fitted profiles tended to be slightly more centrally peaked than H90, which resulted primarily in slightly *lower* inferred $M_*/L_K$ ratios when adopted as mass models. We also experimented with replacing the H90 model with a de Vaucouleurs model (Mellier & Mathez 1987), and adopting $R_{\rm eff}$ values from Pahre (1999).

Elliptical galaxies exhibit radial colour gradients, which may reflect gradients in the metallicity or age of the stellar population (see discussion in § 8.4). These may therefore imply a radial gradient in the stellar M/L ratio. It is beyond the scope of this present work to take such a gradient into account. However, we investigated the sensitivity of our results to the precise shape of the optical light profile we adopted by experimenting with replacing the K-band $R_{\rm eff}$ for each galaxy with the (typically larger) B-band value listed in RC3. For NGC 6482, for which $R_{\rm eff}$ is not listed in RC3, we simply increased $R_{\rm eff}$ by 50%.

### 7.3. *Background subtraction*

One of the major potential sources of systematic uncertainty in measuring the mass profiles of galaxies is the background subtraction technique. This is especially important in the low surface-brightness regime at large radii in our galaxies. In order to estimate the likely magnitude of uncertainty arising from our modelling, when initially fitting the background components (§ 3.1) we artificially adjusted the slope of the instrumental background components, which dominate at high energy, to the limits of their 90% confidence regions, refitting the other components and then refitted all the spectra with these revised background models.

### 7.4. *X-ray asymmetries*

We note that there are some low-level asymmetries in the X-ray surface brightness profiles (§ 4). In order to assess the potential impact of these features, we experimented with excluding or including the features. In particular, we tried excluding data from the vicinity of the jet and AGN in NGC 4261. We also excluded data from an off-axis X-ray asymmetry in NGC 4125 and excluded data for NGC 4472 outside $6'$, where Irwin & Sarazin (1996) pointed out that the X-ray data become asymmetric. These choices did not dramatically affect our results, indicating that these features did not indicate a significant violation of hydrostatic equilibrium, at least in an azimuthally-averaged sense. To gain an insight into possible asymmetries in other sources, we tried re-extracting all our spectra, and re-deriving the mass profiles, from suitably-oriented semi-annuli (thereby excluding one half of the emission from each system).

### 7.5. *Temperature profile*

In principle multiple temperature profiles may be able to fit the same data adequately well but give rise to slightly different global halo parameters. In particular our constraints upon $f_b$, the computation of which requires the extrapolation of the density (and hence temperature) profiles to large radius, may make $M_{\rm vir}$ and c sensitive to this effect. To test this, we experimented with cycling through each of our adopted temperature profiles (eq 3–5). Provided the fits were of comparable quality to our preferred choice, the impact on the best-fit parameters reflect the systematic uncertainty in this choice. Furthermore, we also experimented with excluding the central bin from the temperature profiles of NGC 1407 and NGC 4649, which may indicate a central disturbance (although there is no obvious X-ray morphological disturbance in this region). These choices did not strongly affect our results.

### 7.6. *Spectral-fitting choices*

A variety of choices are made in the spectral-fitting, each of which can affect, to some degree, the inferred $\rho_g$ and temperature in each radial bin. A thorough discussion of these effects is given in Humphrey & Buote (2006).

*Column density.* In order to take account of possible local deviations in the line-of-sight $N_H$ from the value of Dickey & Lockman (1990), we experimented with allowing $N_H$ to vary by ±25%.

*Bandwidth.* To estimate the impact of the bandwidth on our fits, we experimented with fitting the data in the energy ranges 0.7–7.0 keV, 0.5–2.0 keV and 0.4–7.0 keV, in addition to our preferred choice 0.5–7.0 keV.

*Plasma code.* There are some uncertainties in the correct modelling of the individual emission lines, in particular those of Fe. This can systematically lead to differences in the inferred temperature and density depending on choice of plasma code. We therefore experimented with replacing the APEC model with the MEKAL plasma model.

*Unresolved source component.* We included a 7.3 keV bremsstrahlung component to account for unresolved point sources within $D_{25}$. This model is generally a good fit to the resolved point sources in early-type galaxies, but is an empirical result which may not be appropriate to model all unresolved sources in all early-type galaxies. We therefore tested the sensitivity of our results to this model, by replacing the bremsstrahlung component with a simple power law (with $\Gamma$ =1.5) or varying the temperature of the component by ±25%

### 7.7. *Distance uncertainty*

The estimated distance to the object enters into our mass determination (Eq 1) primarily through the impact on the radial scale. To assess its impact on our fitting, we experimented by varying the distance by ±20%.

### 7.8. *Stellar baryon fraction*

In our analysis, we restricted $f_b$ to enable interesting constraints on $M_{vir}$ and c. For the stellar contribution to the baryon fraction, we assumed that mass is divided among group members following the B-band light, which is not formally correct since $M_*/L$ ratios are very sensitive to the age of the stellar population. To estimate how much impact this makes to our fits, we experimented with assuming that all the stellar mass is in the central galaxy, which should place an upper limit on the uncertainty arising from this choice.

## 8. DISCUSSION

### 8.1. *Hydrostatic equilibrium*

Our fit results provide strong evidence that the gas is in hydrostatic equilibrium in these systems. Despite highly nontrivial temperature and density profiles, we were able to recover smooth mass profiles in remarkably good agreement with expectation for these systems, using two complementary techniques. If the gas is significantly out of hydrostatic equilibrium, this would represent a remarkable "conspiracy" between the density and temperature profiles. It is unsurprising that the gas is close to hydrostatic equilibrium in these systems, since we took care to choose objects with relaxed X-ray morphology. Based on N-body/ hydrodynamical analysis, X-ray measurements are expected to give reliable constraints on the DM in systems without obvious substructure (Buote & Tsai 1995).

Further support for hydrostatic equilibrium is provided by the general agreement between our measured $M_*/L_K$ ratios and those predicted by SSP models, coupled with the agreement between the measured $M_{vir}$-c relation and that expected. Similarly a comparison between our results and masses determined from stellar dynamics provides even more evidence that our measured mass profiles are reliable. Dynamically-determined $M_{grav}/L_B$ within the B-band $R_{eff}$ are typically found to be ∼4–10 (Gerhard et al. 2001; Trujillo et al. 2004). We found $M_{grav}/L_B$ within the B-band $R_{eff}$ (taken from RC3 or Faber et al. 1989) for our systems ranged from ∼3 to ∼8, in good agreement with this result. For NGC 4649, outside $R_{eff}$ there is excellent agreement between our measured $M_{grav}/L$ profile and that obtained from globular cluster kinematics, although at small radii the X-ray data lie ∼30% lower (K. Gebhardt et al, in preparation). van der Marel (1991) constructed stellar kinematical models for 5 galaxies in our sample (NGC 720, NGC 1407 and NGC 4261, NGC 4472 and NGC 4649), under the assumption of a constant M/L profile. Strictly speaking a direct comparison cannot be made between their $M_{grav}/L_B$ measurements and our results since our data indicate this assumption is incorrect. However, if we simply assume that these M/L ratios represent those integrated out to $R_{eff}$, the X-ray inferred masses vary from ∼40% lower to ∼10% higher than those from kinematics. Kronawitter et al. (2000) report $M_{grav}/L_B \sim 8\pm1.5$ for NGC 4472 within ∼50″, at which radius our X-ray determined value is ∼50% lower. The discrepancies between the X-ray and dynamical masses are only modest (the X-ray mass being on average ∼20% lower), indicating that the data must be close to hydrostatic equilibrium. Turbulence is expected to contribute only ∼10% pressure support in clusters, which are believed to be more turbulent than galaxies, (Rasia et al. 2006). Therefore, on a case-by-case basis, the observed differences are most likely a manifestation of the mass-anisotropy degeneracy (e.g. Dekel et al. 2005).

### 8.2. *Mass profiles*

We obtained detailed mass profiles for 3 galaxies and 4 group-scale systems, out to ∼10$R_{eff}$. The data clearly show M/L profiles which are ∼flat within $R_{eff}$ and rise considerably outside this range. This confirms the presence of substantial DM in at least some early-type galaxies and indicates that a stellar mass component dominates within ∼$R_{eff}$. This is consistent with studies of stellar kinematics and similar to the mass decomposition analysis of Brighenti & Mathews (1997).

The data are well-fitted by a model comprising a stellar mass (H90) component and an NFW DM profile. Omitting the stellar mass component led to systematically poorer fits, smaller $M_{vir}$ and vastly larger c ($\gg$20), which are inconsistent with the predictions of ΛCDM. This effect is easy to understand— if we add a compact stellar mass component to an (extended) NFW profile, we increase the mass in the core which, by definition, makes the halo more concentrated. However, it is not entirely clear whether this effect, pointed out by Mamon & Łokas (2005), can completely account for the significantly steeper $M_{vir}$-c relation found by Sato et al. (2000). Based on our analysis of group-scale halos (Gastaldello et al. 2006) we found that the inclusion of the stellar mass component does not have a strong effect on c in most systems with $M_{vir} \gtrsim 2\times10^{13} M_\odot$, provided the data are fitted to a sufficiently large fraction of $R_{vir}$. The data did not allow us to distinguish statistically between the simple NFW+stars model and scenarios in which the DM halo experiences adiabatic compression due to star formation (however, see § 8.4), or the NFW profile was replaced with the alternative N04 profile.

Comparing our inferred $M_{vir}$ and c to the predictions of ΛCDM we find general agreement. There is some evidence, however, that the concentrations are systematically higher than one would expect, although the errorbars are typically large. Such a trend is also seen in our analysis of groups (Gastaldello et al. 2006). Whilst the slope of the $M_{vir}$-c relation therefore implied by our data is difficult to explain by varying the cosmological parameters within reasonable limits (Buote et al. 2006a), we suspect that the discrepancy can be resolved by taking into account the selection function of our galaxies.

Our data were not selected in a statistically complete manner and, by choosing objects with relatively relaxed X-ray morphologies we are probably selecting objects which have not had a recent major merger. This systematically biases us towards early-forming, hence higher concentration halos. In fact, it is striking that all three *de facto* galaxies in our sample are relatively isolated systems (§ 8.3). Such systems preferentially might be expected to occupy high-c halos (Zentner et al. 2005),

which does appear to be the case for 2 out of 3 of the galaxies. We will return to these issues in detail in Buote et al. (2006a).

### 8.3. *Galaxies, Groups and Fossil Groups*

All three of the lowest-mass systems in our sample are very isolated optically. NGC 6482 matches the isolation criteria adopted to identify so-called "fossil groups" (Khosroshahi et al. 2004). NGC 4125 and NGC 720 are both listed as "groups" in G93, but closer inspection actually reveals they are also very isolated. Excepting the central galaxy, only one of the putative members of the NGC 720 "group" listed in the G93 catalogue (which omits the dwarf galaxy population studied by Dressler et al. 1986), actually lies within the projected $R_{vir}$ (but outside $0.75\times R_{vir}$) and it is 2.4 magnitudes fainter in B than the central galaxy. Dressler et al. remarked upon the optical isolation of this galaxy. Of the two putative companion galaxies to NGC 4125 given in G93 which lie within the projected $R_{vir}$ (but outside $0.67\times R_{vir}$), both are much fainter (by 2.3 and 3.9 magnitudes, respectively) in B than the central galaxy. In contrast, the four remaining systems in our sample are much less optically isolated. Schindler et al. (1999) show the clear over-density of early-type galaxies around NGC 4649 and NGC 4472, and almost 60 group members are associated with these systems by G93. Gould (1993) identified at least 10 members of the NGC 1407 group, from the dynamics of which he inferred a mass broadly consistent with our measured $M_{vir}$ (§ 8.7). Helsdon & Ponman (2003) report 57 galaxies associated with the NGC 4261 group within ∼1 Mpc projected radius, which is consistent with our measured $R_{vir}$.

Rather than an isolated galaxy Khosroshahi et al. (2004) identify NGC 6482 as a "fossil group". Fossil groups are group-sized X-ray halos centred on essentially a single elliptical galaxy (Ponman et al. 1994; Vikhlinin et al. 1999; Jones et al. 2003). The typical interpretation of these objects is groups in which all of the $L_*$ members have merged. Confusingly, using almost the same selection criteria, O'Sullivan & Ponman (2004) classify the galaxy NGC 4555 as an "isolated elliptical galaxy" and posit a very different formation scenario. This object appears to be more massive than NGC 6482; the authors found $M_{grav}\sim 3\times10^{12}M_\odot$ within 60 kpc which, assuming an NFW profile with c=15 would imply $M_{vir}\sim 2\times10^{13}M_\odot$. Nonetheless, both of these systems have more in common (both optically and in the X-ray) with each other, and the other isolated ellipticals in our sample, than, for example, the massive ($M_{vir}\gtrsim10^{14}M_\odot$), hotter (kT∼2 keV) fossil groups considered by Vikhlinin et al. (1999). We suspect that the distinction made between "isolated elliptical" and "fossil group" for these two systems is largely semantic, and consider NGC 6482 more properly an isolated galaxy, too.

The clear division in the galaxy content of our sample clearly lends itself to the nomenclature "galaxies" for the three lowest-mass systems, and "groups" for the others. Strikingly, this separation between galaxies and groups also appears consistent with a difference in temperature profiles (§ 8.6). That this distinction appears commensurate with $M_{vir}\sim10^{13}M_\odot$ is suggestive that this mass-scale may be a useful yard-stick with which to compare to other systems. The error-bars on our mass estimates are sufficiently large that the 90% confidence regions of several of the objects (notably NGC 720, NGC 6482 and NGC 1407) actually straddle $10^{13}M_\odot$. However, it is clear that *on average*, the systems with $M_{vir}\lesssim10^{13}M_\odot$ are galaxies. We note that the $M_{vir}$ adopted here is that *before* any tidal truncation which is almost certainly occurring as NGC 4472 and NGC 4649 merge with Virgo (their untruncated $R_{vir}$ would stretch much of the distance to M 87). $M_{vir}$ does not exactly correlate with formation epoch, so that lower-mass halos may still be in the process of forming (hence contain multiple galaxies of similar magnitude), and more massive halos may contain single, dominant ellipticals (fossil groups). Nonetheless, classifying halos primarily on the basis of $M_{vir}$ provides a straightforward way to locate them in the formation hierarchy. Traditionally, galaxy-like and group-like systems are distinguished on the basis of local over-densities of galaxies. However, placing optically-identified groups into a cosmological context requires a firm understanding not only of the formation of DM halos but also how galaxies populate them, which is much less well-understood (e.g. Kravtsov et al. 2004). This problem is compounded by the difficulties faced by optical group-finding algorithms in identifying very poor groups (e.g. Gerke et al. 2005). Not only can a significant fraction of putative groups be chance superpositions of galaxies, particularly along filaments, but adjacent groups can be merged, such as happened for NGC 4649 and NGC 4472 in G93. If there are only a few identified members, small-number statistics and the treatment of interlopers can affect their interpretation (e.g. Gould 1993). To complicate matters further, some authors refer to *any* over-density of galaxies as a group, even a Milky Way-sized galaxy and its dwarf satellites (e.g. Tully 2005).

### 8.4. *Stellar Mass-to-Light Ratios*

Comparing our measured stellar M/L ratios to the predictions of simple stellar population (SSP) models, we found reasonable agreement provided one assumes a Kroupa (2001) IMF. There is modest disagreement, even when the less-cuspy N04 DM model was adopted. Considering the uncertainties in the SSP modelling (discussed below), however, we believe this discrepancy is not significant. If we allowed the DM profile to be modified by adiabatic compression, we obtained substantially smaller $M_*/L_K$ values from our data, (since it increases the cuspiness of the halo) which are more discrepant with the SSP models. This result casts doubt on AC being as significant an effect as currently modelled. However, the data alone did not allow us statistically to distinguish between the NFW+stars and AC NFW+stars models. Nonetheless, this result is joining a growing body of literature which similarly calls into question whether AC operates as predicted (Zappacosta et al. 2006; Kassin et al. 2006; Sand et al. 2004).

There are a number of major uncertainties in the computation of the stellar mass-to-light ratios from the SSP models. Specifically, the results are very dependent upon the assumed IMF, which is not confidently known in early-type galaxies. Furthermore there is some evidence that early-type galaxies frequently contain multiple stellar populations of different ages, including a significant young population (e.g. Rembold et al. 2005; Nolan et al. 2006). Depending on the mass fraction of the young

component, this may substantially reduce $M_*/L_K$ in the galaxy, hence possibly reconciling the data and the AC NFW+stars model. A small amount of star formation may also give rise to a population of stars which can dominate the light in the galaxy core, giving rise to significantly lower synthetic $M_*/L_K$ than measured. This may be the case in NGC 720 (see § 6.5). More problematically, there are known to be significant abundance, or possible age, gradients in the stellar populations of early-type galaxies (e.g. Trager et al. 2000; Kobayashi & Arimoto 1999; Rembold et al. 2005), which would translate into stellar $M_*/L_K$ gradients. Our simple modelling did not allow us to account for such an effect *per se*. Although we suspect that such gradients will primarily lead to a $M_*/L_K$ value which reflects an average for the galaxy, $M_*/L_K$ does depend to some extent upon the shape of the assumed stellar potential. Properly taking account of this effect is beyond the scope of this present work, but may bring the synthetic M/L ratios and our results into better agreement. Clearly this is only one of a number of other systematic effects which may also reconcile the slight discrepancy (Table 6).

### 8.5. *Baryon fractions*

An interesting result from our analysis is that these systems, despite having masses $\gtrsim 5\times10^{12}M_\odot$, do not appear in general to be baryonically closed. To some extent this trend was enforced by applying Eq 6 to constrain the data. However, the excellent fits we obtained by this method, in conjunction with the good agreement between the measured $M_{vir}$-c relation and the predictions of ΛCDM and, crucially, our measurements at the group scale (which do not employ this restriction: Gastaldello et al. 2006), indicate that the inferred $f_b$(∼0.04–0.09; Table 4) are accurate. Furthermore, if we relaxed this constraint and instead restricted $f_b$ to a finite range, we also found that the data tended to favour modest values of $f_b$. In particular, for any given system, the measured $M_{vir}$ and $f_b$ were strongly anti-correlated, so that our upper $M_{vir}$ constraint is in part imposed by the *lower* limit we place on $f_b$. Given the shapes of the $M_{vir}$-c contours (Fig 4), it is clear that good agreement with the $M_{vir}$-c relation predicted from simulations tends, therefore, to require rather modest values of $f_b$. This would suggest that strong feedback plays an important role in the evolution of these objects.

### 8.6. *Temperature profiles*

By inspection of the temperature profiles (Fig 2) it is immediately clear that, for all of the galaxy-scale systems in our sample the temperature profiles have negative gradients. In contrast the group-scale objects have positive temperature gradients, similar to observations of other X-ray bright groups and clusters (Gastaldello et al. 2006; Vikhlinin et al. 2005; Piffaretti et al. 2005). This radical difference in the temperature profiles seems consistent with our division of galaxies and groups at $M_{vir}\sim 10^{13}M_\odot$. The origin of this distinct demarcation between objects around $10^{13}M_\odot$ is unclear, however. Negative temperature gradients are expected for isolated galaxies containing relatively cool gas, such as that arising from stellar mass-loss. In the deep stellar potential well, compressive heating of the gradually inflowing gas can dominate over radiative cooling to produce a negative temperature slope. In contrast, if hotter (∼1–2 keV) baryons are allowed to flow in, radiative cooling dominates to produce a positive temperature gradient (Mathews & Brighenti 2003). It is by no means clear, however, why the hot baryons appear to be present only in the systems with $M_{vir}\gtrsim 10^{13}M_\odot$. One possibility is the local environment; all of the galaxy-scale objects are rather isolated, whereas the groups NGC 4472 and NGC 4649, in particular, are found in a relatively dense cluster environment, which could provide a reservoir of hot baryons. However, such an explanation cannot easily account for the positive temperature gradient in NGC 1407, which is comparatively isolated, or the isolated system NGC 4555, which appears only slightly more massive than our galaxies.

It is possible that selection effects may have played some role in the bimodal temperature profile behaviour, since both NGC 4125 and NGC 6482 are classified in *NED* as LINERS, and NGC 720 has a dominant young stellar population (Appendix A). However, none of these systems show strong X-ray morphology disturbances in the core, which might indicate a substantial energy input from star-formation or AGN activity. In any case, the cooling time in the core of NGC 720 is only ∼200 Myr, substantially less than the implied time since the last major burst of star formation, and so the negative temperature gradient cannot simply be related to energy injection during a starburst. Furthermore, at least two of the group-scale systems also harbour AGN and do not show obvious negative temperature gradients in the core.

Another example of an object we believe to be a galaxy (rather than a group) which exhibits a negative temperature gradient is the S0 NGC 1332 (Humphrey et al. 2004). A possible counter-example to this trend might by the "isolated elliptical galaxy" NGC 4555, which exhibits a temperature profile akin to the groups in our sample (O'Sullivan & Ponman 2004). However, as we discuss in § 8.3, this probably has comparable $M_{vir}$ to the groups.

Another intriguing feature of two of the group scale objects is a central temperature peak, similar to a feature we found in the cluster A 644 (Buote et al. 2005). In that system, we found a significant offset between the X-ray centroid and the emission peak in an otherwise fairly relaxed object. We suggested that both of these features may be related to the cD "sloshing" in the potential well of the cluster, which is relaxing following disturbance by, for example, a merger. We do not find obvious evidence of a similar offset in either NGC 1407 or NGC 4649. However, these groups may be in a comparably more relaxed (evolved) state than A 644. Alternatively, the central peaks may be related to past AGN activity heating the gas in the core of the galaxies, from which the system has had time to relax dynamically but not cool completely.

### 8.7. *Is NGC 1407 a "dark group"?*

Based on the group member dispersion velocity Gould (1993) suggested that NGC 1407 may lie in a massive ($\gtrsim$ a few $\times10^{13}M_\odot$) DM halo. Although such a conclusion was strongly dependent on the association of the galaxy NGC 1400, which exhibits a large peculiar velocity, with the group, we can now confirm the presence of a substantial DM halo around this system. Both the temperature profile and our best-fit mass are similar to

the bright X-ray group NGC 5044 (Buote et al. 2006b), and yet it is almost 2 orders of magnitude fainter in $L_X$. NGC 5044 appears to be close to baryonic closure (Mathews et al. 2005), and so has likely retained most of its large gaseous halo. On the other hand NGC 1407 is not baryonically closed (we estimate $f_b \simeq 0.06$) and so the loss of much of its hot gas envelope easily explains its lower $L_X/L_B$. Since the masses of the two systems are not considerably different, this points to substantial variation in the evolutionary history of these two groups. In particular, feedback may have operated more efficiently in evacuating the gas from NGC 1407.

Gould's preferred mass estimate ($\sim 10^{14} M_\odot$) would imply a remarkably high M/L ratio for the system ($M_{vir}/L_B \sim 900 M_\odot/L_\odot$), making NGC 1407 a bona fide "dark group". The existence of such an object would provide a valuable insight into the process of star formation in DM halos, as it would imply star formation was somehow inhibited in that system. This mass estimate is, however, considerably larger than our preferred value $\sim 1.5 \times 10^{13} M_\odot$, which implies a more modest M/L ratio ($M_{vir}/L_B \sim 140 M_\odot/L_\odot$). To some extent, though, our constraint on $f_b$, which was necessary to obtain interesting $M_{vir}$ constraints, has probably enforced this behaviour. Such a restriction may not be valid in a system with an unusual star-formation history and so we experimented with freeing $f_b$. To enable $M_{vir}$ to be constrained, we restricted c to lie on the best-fit $M_{vir}$-c relation found by Bullock et al. (2001). The best-fitting mass, $M_{vir} = (9.7^{+17.8}_{-6.2}) \times 10^{13} M_\odot$, was in good agreement with Gould (1993)'s values, but implies a baryon fraction only of $\sim 0.003$. Since this fit was statistically indistinguishable from the preferred model, we cannot determine which mass estimate is more likely.

## 9. SUMMARY

Using *Chandra* we have obtained detailed mass profiles centred on 7 elliptical galaxies, of which 3 were found to have *de facto* galaxy-scale halos, with $M_{vir} < 10^{13} M_\odot$, and 4 had group-scale ($10^{13} M_\odot < M_{vir} < 10^{14} M_\odot$) halos. These represent the best available data for nearby objects with comparable $L_X$. In summary:

1. The M/L ratio profiles were $\sim$flat within $R_{eff}$ and rose sharply outside this region, indicating substantial DM in all 7 systems.

2. The data were well-described by a two component model, comprising an NFW potential for the DM and a H90 stellar mass model. We were not able statistically to distinguish between this scenario and one in which the DM profile was modified by "adiabatic compression" due to baryonic infall. Similarly, we could not distinguish between the NFW and the revised N04 DM halo profiles.

3. The distribution of the galaxies in the $M_{vir}$-c plane was in broad agreement with the predictions of $\Lambda$CDM, although with a slight trend toward more concentrated halos, in good agreement with our modelling of X-ray bright groups and poor clusters (Gastaldello et al. 2006). This probably represents a galaxy selection bias to earlier-forming systems, and we will discuss how we might account for it in Buote et al. (2006a). Allowing AC to modify the shape of the DM halo did not appreciably affect the $M_{vir}$-c relation.

4. Omitting the stellar mass component resulted in systematically poorer fits, smaller $M_{vir}$ and unphysically large c, confirming the conclusions of Mamon & Łokas (2005). This may explain very large values of c found by some previous X-ray observers (e.g. Sato et al. 2000; Khosroshahi et al. 2004).

5. For the NFW+stars model, $M_*/L_K$ was found to be in approximate agreement with the predictions of simple stellar population synthesis models, assuming a Kroupa (2001) IMF. The AC NFW+stars models have significantly lower $M_*/L_K$ which seems to cast doubt on the AC scenario, although this conclusion is sensitive to the considerable uncertainties in the theoretical modelling.

6. Despite having $M_{vir} \gtrsim 5 \times 10^{12} M_\odot$, typically $f_b \sim 0.04$–$0.09$ for each galaxy, implying that feedback has played an important role in the evolution of these systems.

7. The temperature profiles of the galaxy-scale systems all exhibited negative radial gradients, whereas the group-scale objects exhibited positive gradients, similar to the "Universal" temperature profiles being found in other X-ray bright groups and clusters. This implies a strict line of demarcation between systems at $M_{vir} \sim 10^{13} M_\odot$.

8. In two of the groups, we found central temperature peaks, similar to that found in the cluster A 644 (Buote et al. 2005), but no obvious central disturbances in X-ray morphology. This may relate to past AGN activity, following which the heated gas in the core of the galaxy has relaxed but not cooled.

9. We confirm the suggestion of Gould (1993) that the elliptical galaxy NGC 1407 lies at the centre of a massive DM halo, possibly making it a "dark group" with an unusually large M/L. Our best-fitting $M_{vir}$ is considerably lower than that of Gould, implying M/L more consistent with normal groups. Nonetheless, if we relax the assumptions of our modelling very large masses ($M_{vir} \sim 10^{14} M_\odot$) are allowed.

We would like to thank Oleg Gnedin for making available his adiabatic compression code. We would also like to thank Karl Gebhardt for communicating with us results from his paper in preparation. We thank Louisa Nolan for interesting discussions on the stellar populations of galaxies. This research has made use of data obtained from the High Energy Astrophysics Science Archive Research Center (HEASARC), provided by NASA's Goddard Space Flight Center. This research has also made use of the NASA/IPAC Extragalactic Database (*NED*) which is operated by the Jet Propulsion Laboratory, California Institute of Technology, under contract with NASA. In addition, this work also made use of the HyperLEDA database (http://leda.univ-lyon1.fr). Support for this work was provided by NASA

TABLE A7
Stellar population parameters

| Galaxy | indices | ref. | [$\alpha$/Fe] | age (Gyr) | [Z/H]$_0$ | $<$ [Z/H] $>$ |
|---|---|---|---|---|---|---|
| NGC 720$^\dagger$ | H$\beta$, Mgb, Fe5270, Fe5335 | 2 | 0.37±0.05 | $2.9^{+1.3}_{-0.3}$ | 0.65±0.13 | 0.48±0.18 |
| NGC 1407$^\dagger$ | H$\beta$, Mgb, Fe5270, Fe5335 | 1 | 0.33±0.02 | 12±2 | 0.35±0.06 | 0.08±0.06‡ |
| NGC 4125 | H$\beta$, Mgb, Fe5270, Fe5335 | 3 | 0.33±0.16 | 13±8 | 0.16±0.25 | -0.11±0.25‡ |
| NGC 4261 | H$\beta$, Mgb, Fe5270, Fe5335 | 2 | 0.25±0.02 | 15±1 | 0.30±0.03 | -0.03±0.10 |
| NGC 4472$^\dagger$ | H$\beta$, Mgb, Fe5270, Fe5335 | 2 | 0.25±0.03 | 9±2 | 0.36±0.05 | 0.17±0.12 |
| NGC 4649 | H$\beta$, Mgb, Fe5335 | 2 | 0.25±0.02 | 13±2 | 0.41±0.04 | 0.23±0.15 |
| NGC 6482 | Mgb, Fe5270, Fe5335 | 3 | 0.30±0.15 | 12 | 0.28±0.15 | 0.06±0.15‡ |

Note. — Stellar population parameters determined from Lick index fitting. The indices used in fitting are listed (indices), as is the reference (ref) whence they were taken. Those mean stellar abundances ($<$ [Z/H] $>$) marked ‡ were estimated from the central abundance ([Z/H]$_0$) adopting the mean abundance gradient [Z/H]$_0$ − $<$ [Z/H] $>$ = 0.27(see Humphrey & Buote 2006). Where no error-bar is given, the parameter was frozen. Table references: 1— Beuing et al. (2002), 2— Trager et al. (2000), 3— Trager et al. (1998) Results for galaxies marked $^\dagger$ were taken from Humphrey & Buote (2006)

under grant NNG04GE76G issued through the Office of Space Sciences Long-Term Space Astrophysics Program.

## APPENDIX

## STELLAR POPULATION PARAMETERS

The mass-to-light ratio of a stellar population is dependent upon both the age and the metal abundance ([Z/H]) of the stars. To estimate these quantities we searched the literature to obtain Lick/IDS indices for each galaxy, which we fitted with the simple stellar population (SSP) models of Thomas et al. (2003), using the technique outlined in Humphrey & Buote (2006). Briefly, we constructed a model by linearly interpolating the SSP models as a function of stellar age, metallicity and $\alpha$-element to Fe ratio, which was then fitted *via* a $\chi^2$ minimization technique to those indices shown in Table A7. Trager et al. (2000) provided indices measured in two apertures, which enabled us to take account of any abundance gradients, as outlined in Humphrey & Buote (2006). Where only a central Lick index was available, we estimated the total emission-weighted abundance by correcting the central metallicity by -0.27 dex. We did not attempt to take account of possible age gradients. The results, including the Lick indices adopted and the reference whence the indices were obtained, are shown in Table A7. This method implicitly assumes that all the stars were created in a single burst of star formation, which may be over-simplistic if there are, in fact, multiple bursts of star formation in early-type galaxies (e.g. Rembold et al. 2005; Nolan et al. 2006). We note that we were not able to obtain acceptable solutions for NGC 6482 if we used the H$\beta$ index, which is the most sensitive age indicator. This galaxy is classified in *NED* as a LINER and is rather blue for an old stellar population ($M_B - M_K = 3.4 \pm 0.2$, whereas a 12 Gyr, solar abundance population is expected to have $M_B - M_K \simeq 3.9$: Maraston 1998). Both of these factors might suggest the presence of a significant young population of stars (although see Cid Fernandes et al. 2004). It is beyond the scope of this present work, however, to attempt to take account of this effect.

## REFERENCES


Asplund, M., Grevesse, N., & Sauval, J. 2004, in Cosmic abundances as records of stellar evolution and nucleosynthesis, ed. F. N. Bash & T. G. Barnes (ASP Conf. series), astro-ph/0410214

Bailin, J., Power, C., Gibson, B. K., & Steinmetz, M. 2005, MNRAS, submitted, astro-ph/0502231

Bergond, G., Zepf, S. E., Romanowsky, A. J., Sharples, R. M., & Rhode, K. L. 2006, A&A, 448, 155

Beuing, J., Bender, R., Mendes de Oliveira, C., Thomas, D., & Maraston, C. 2002, A&A, 395, 431

Binney, J. J., Davies, R. L., & Illingworth, G. D. 1990, ApJ, 361, 78

Blumenthal, G. R., Faber, S. M., Flores, R., & Primack, J. R. 1986, ApJ, 301, 27

Borriello, A., Salucci, P., & Danese, L. 2003, MNRAS, 341, 1109

Brighenti, F. & Mathews, W. G. 1997, ApJ, 486, L83+

Brown, R. J. N., Forbes, D. A., Silva, D., Helsdon, S. F., Ponman, T. J., Hau, G. K. T., Brodie, J. P., Goudfrooij, P., & Bothun, G. 2003, MNRAS, 341, 747

Bullock, J. S., Kolatt, T. S., Sigad, Y., Somerville, R. S., Kravtsov, A. V., Klypin, A. A., Primack, J. R., & Dekel, A. 2001, MNRAS, 321, 559

Buote, D. A. 2000, ApJ, 539, 172

Buote, D. A., Brighenti, F., & Mathews, W. G. 2004, ApJ, 607, L91

Buote, D. A., Bullock, J. S., Gastaldello, F., Humphrey, P. J., Zappacosta, L., Brighenti, F., & Mathews, W. G. 2006a, in preparation

Buote, D. A. & Canizares, C. R. 1994, ApJ, 427, 86

Buote, D. A. & Canizares, C. R. 1996, ApJ, 457, 177

Buote, D. A. & Canizares, C. R. 1998, MNRAS, 298, 811

Buote, D. A., Gastaldello, F., Humphrey, P. J., Zappacosta, L., Bullock, J. S., Brighenti, F., & Mathews, W. G. 2006b, in preparation

Buote, D. A., Humphrey, P. J., & Stocke, J. T. 2005, ApJ, 630, 750

Buote, D. A., Jeltema, T. E., Canizares, C. R., & Garmire, G. P. 2002, ApJ, 577, 183

Buote, D. A., Lewis, A. D., Brighenti, F., & Mathews, W. G. 2003, ApJ, 594, 741

Buote, D. A. & Tsai, J. C. 1995, ApJ, 439, 29

Carpenter, J. M. 2001, AJ, 121, 2851

Cembranos, J. A., Feng, J. L., Rajaraman, A., & Takayama, F. 2005, Physical Review Letters, 95, 181301

Cid Fernandes, R., González Delgado, R. M., Schmitt, H., Storchi-Bergmann, T., Martins, L. P., Pérez, E., Heckman, T., Leitherer, C., & Schaerer, D. 2004, ApJ, 605, 105
Croston, J. H., Hardcastle, M. J., & Birkinshaw, M. 2005, MNRAS, 357, 279
de Vaucouleurs, G., de Vaucouleurs, A., Corwin, H. G., Buta, R. J., Paturel, G., & Fouque, P. 1991, Third Reference Catalogue of Bright Galaxies (Volume 1-3, XII, 2069 pp. 7 figs.. Springer-Verlag Berlin Heidelberg New York)
Dekel, A., Stoehr, F., Mamon, G. A., Cox, T. J., Novak, G. S., & Primack, J. R. 2005, Nature, 437, 707
Dickey, J. M. & Lockman, F. J. 1990, ARA&A, 28, 215
Diemand, J., Zemp, M., Moore, B., Stadel, J., & Carollo, M. 2005, MNRAS, 364, 665
Dressler, A., Schechter, P. L., & Rose, J. A. 1986, AJ, 91, 1058
El-Zant, A. A., Hoffman, Y., Primack, J., & Combes, F. a nd Shlosman, I. 2004, ApJ, 607, L75
Faber, S. M., Wegner, G., Burstein, D., Davies, R. L., Dressler, A., Lynden-Bell, D., & Terlevich, R. J. 1989, ApJS, 69, 763
Fischer, P., et al. 2000, AJ, 120, 1198
Forman, W., Jones, C., & Tucker, W. 1985, ApJ, 293, 102
Freeman, P. E., Kashyap, V., Rosner, R., & Lamb, D. Q. 2002, ApJS, 138, 185
Fukazawa, Y., Botoya-Nonesa, J. G., Pu, J., Ohto, A., & Kawano, N. 2006, ApJ, 636, 698
Garcia, A. M. 1993, A&AS, 100, 47
Gastaldello, F., Buote, D. A., Humphrey, P. J., Zappacosta, L., Bullock, J. S., Brighenti, F., & Mathews, W. G. 2006, in preparation
Gerhard, O., Kronawitter, A., Saglia, R. P., & Bender, R. 2001, AJ, 121, 1936
Gerke, B. F., et al. 2005, ApJ, 625, 6
Gnedin, O. Y., Kravtsov, A. V., Klypin, A. A., & Nagai, D. 2004, ApJ, 616, 16
Gonzalez, A. H., Williams, K. A., Bullock, J. S., Kolatt, T. S., & Primack, J. R. 2000, ApJ, 528, 145
Gould, A. 1993, ApJ, 403, 37
Helsdon, S. F. & Ponman, T. J. 2003, MNRAS, 340, 485
Hernquist, L. 1990, ApJ, 356, 359
Hogan, C. J. & Dalcanton, J. J. 2000, Phys. Rev. D, 62, 063511
Humphrey, P. J. & Buote, D. A. 2004, ApJ, 612, 848
Humphrey, P. J. & Buote, D. A. 2006, ApJ, 639, 136
Humphrey, P. J., Buote, D. A., & Canizares, C. R. 2004, ApJ, 617, 1047
Humphrey, P. J., Buote, D. A., Gastaldello, F., Zappacosta, L., Bullock, J. S., Brighenti, F., & Mathews, W. G. 2005, in The X-Ray Universe 2005
Irwin, J. A., Athey, A. E., & Bregman, J. N. 2003, ApJ, 587, 356
Irwin, J. A. & Sarazin, C. L. 1996, ApJ, 471, 683
Jensen, J. B., Tonry, J. L., Barris, B. J., Thompson, R. I., Liu, M. C., Rieke, M. J., Ajhar, E. A., & Blakeslee, J. P. 2003, ApJ, 583, 712
Jing, Y. P. 2000, ApJ, 535, 30
Jones, C., Forman, W., Vikhlinin, A., Markevitch, M., David, L., Warmflash, A., Murray, S., & Nulsen, P. E. J. 2002, ApJ, 567, L115
Jones, L. R., Ponman, T. J., Horton, A., Babul, A., Ebeling, H., & Burke, D. J. 2003, MNRAS, 343, 627
Kaplinghat, M. 2005, Phys. Rev. D, 72, 063510
Kassin, S. A., de Jong, R. S., & Weiner, B. J. 2006, ApJ, in press, astro-ph/0602027
Kay, S. T., Thomas, P. A., & Theuns, T. 2003, MNRAS, 343, 608
Khosroshahi, H. G., Jones, L. R., & Ponman, T. J. 2004, MNRAS, 349, 1240
Kim, D. & Fabbiano, G. 2004, ApJ, 611, 846
Kobayashi, C. & Arimoto, N. 1999, ApJ, 527, 573
Kochanek, C. S. 1995, ApJ, 445, 559
Kravtsov, A. V., Berlind, A. A., Wechsler, R. H., Klypin, A. A., Gottlöber, S., Allgood, B., & Primack, J. R. 2004, ApJ, 609, 35
Kronawitter, A., Saglia, R. P., Gerhard, O., & Bender, R. 2000, A&AS, 144, 53
Kroupa, P. 2001, MNRAS, 322, 231
Kuhlen, M., Strigari, L. E., Zentner, A. R., Bullock, J. S., & Primack, J. R. 2005, MNRAS, 357, 387
Lewis, A. D., Buote, D. A., & Stocke, J. T. 2003, ApJ, 586, 135
Loeb, A. & Peebles, P. J. E. 2003, ApJ, 589, 29
Loewenstein, M. & White, R. E. 1999, ApJ, 518, 50
Mamon, G. A. & Łokas, E. L. 2005, MNRAS, 362, 95
Maraston, C. 1998, MNRAS, 300, 872
Markevitch, M. 2002, astro-ph/0205333
Mathews, W. G. & Brighenti, F. 2003, ARA&A, 41, 191
Mathews, W. G., Faltenbacher, A., Brighenti, F., & Buote, D. A. 2005, ApJ, 634, L137
Mellier, Y. & Mathez, G. 1987, A&A, 175, 1
Napolitano, N. R., Capaccioli, M., Romanowsky, A. J., Douglas, N. G., Merrifield, M. R., Kuijken, K., Arnaboldi, M., Gerhard, O., & Freeman, K. C. 2005, MNRAS, 357, 691
Navarro, J. F., Frenk, C. S., & White, S. D. M. 1997, ApJ, 490, 493
Navarro, J. F., Hayashi, E., Power, C., Jenkins, A. R., Frenk, C. S., White, S. D. M., Springel, V., Stadel, J., & Quinn, T. R. 2004, MNRAS, 349, 1039
Nolan, L. A., Harva, M. O., Kabán, A., & Raychaudhury, S. 2006, MNRAS, 366, 321
O'Sullivan, E., Forbes, D. A., & Ponman, T. J. 2001, MNRAS, 328, 461
O'Sullivan, E. & Ponman, T. J. 2004, MNRAS, 354, 935
O'Sullivan, E., Ponman, T. J., & Collins, R. S. 2003, MNRAS, 340, 1375
Padmanabhan, N., et al. 2004, New Astronomy, 9, 329
Pahre, M. A. 1999, ApJS, 124, 127
Perlmutter, S., et al. 1999, ApJ, 517, 565
Pierce, M., et al. 2006, MNRAS, 366, 1253
Piffaretti, R., Jetzer, P., Kaastra, J. S., & Tamura, T. 2005, A&A, 433, 101
Pointecouteau, E., Arnaud, M., & Pratt, G. W. 2005, A&A, 435, 1
Ponman, T. J., Allan, D. J., Jones, L. R., Merrifield, M., McHardy, I. M., Lehto, H. J., & Luppino, G. A. 1994, Nature, 369, 462
Prugniel, P. & Simien, F. 1997, A&A, 321, 111
Randall, S. W., Sarazin, C. L., & Irwin, J. A. 2004, ApJ, 600, 729
Randall, S. W., Sarazin, C. L., & Irwin, J. A. 2006, ApJ, 636, 200
Rasia, E., Ettori, S., Moscardini, L., Mazzotta, P., Borgani, S., Dolag, K., Tormen, G., Cheng, L. M., & Diaferio, A. 2006, MNRAS, submitted, astro-ph/0602434
Rembold, S. B., Pastoriza, M. G., & Bruzual, G. 2005, A&A, 436, 57
Romanowsky, A. J. 2005, in Mass Profiles and Shapes of Cosmological Structures, Proc of XXIst IAP Colloquium, Paris 4–9 July, ed. G. A. Mamon
Romanowsky, A. J., Douglas, N. G., Arnaboldi, M., Kuijken, K., Merrifield, M. R., Napolitano, N. R., Capaccioli, M., & Freeman, K. C. 2003, Science, 301, 1696
Rusin, D., Kochanek, C. S., & Keeton, C. R. 2003, ApJ, 595, 29
Rusin, D., Norbury, M., Biggs, A. D., Marlow, D. R., Jackson, N. J., Browne, I. W. A., Wilkinson, P. N., & Myers, S. T. 2002, MNRAS, 330, 205
Sand, D. J., Treu, T., Smith, G. P., & Ellis, R. S. 2004, ApJ, 604, 88
Sato, S., Akimoto, F., Furuzawa, A., Tawara, Y., Watanabe, M., & Kumai, Y. 2000, ApJ, 537, L73
Schindler, S., Binggeli, B., & Böhringer, H. 1999, A&A, 343, 420
Simon, J. D., Bolatto, A. D., Leroy, A., Blitz, L., & Gates, E. L. 2005, ApJ, 621, 757
Spergel, D. N. & Steinhardt, P. J. 2000, Physical Review Letters, 84, 3760
Spergel, D. N., et al. 2003, ApJS, 148, 175
Statler, T. S., Dejonghe, H., & Smecker-Hane, T. 1999, AJ, 117, 126
Swaters, R. A., Madore, B. F., & Trewhella, M. 2000, ApJ, 531, L107
Swaters, R. A., Verheijen, M. A. W., Bershady, M. A., & Andersen, D. R. 2003, ApJ, 587, L19
Thomas, D., Maraston, C., & Bender, R. 2003, MNRAS, 339, 897
Tonry, J. L., Dressler, A., Blakeslee, J. P., Ajhar, E. A., Fletcher, A. ., Luppino, G. A., Metzger, M. R., & Moore, C. B. 2001, ApJ, 546, 681
Trager, S. C., Faber, S. M., Worthey, G., & González, J. J. . 2000, AJ, 119, 1645
Trager, S. C., Worthey, G., Faber, S. M., Burstein, D., & Gonzalez, J. J. 1998, ApJS, 116, 1
Treu, T. & Koopmans, L. V. E. 2004, ApJ, 611, 739
Trujillo, I., Burkert, A., & Bell, E. F. 2004, ApJ, 600, L39
Tully, R. B. 2005, ApJ, 618, 214
van der Marel, R. P. 1991, MNRAS, 253, 710

Vikhlinin, A., Kravtsov, A., Forman, W., Jones, C., Markevitch, M., Murray, S. S., & Van Speybroeck, L. 2005, ApJ, submitted, astro-ph/0507092
Vikhlinin, A., McNamara, B. R., Hornstrup, A., Quintana, H., Forman, W., Jones, C., & Way, M. 1999, ApJ, 520, L1
Wechsler, R. H., Bullock, J. S., Primack, J. R., Kravtsov, A. V., & Dekel, A. 2002, ApJ, 568, 52
Wechsler, R. H., Zentner, A. R., Bullock, J. S., & Kravtsov, A. V. 2005, ApJ, submitted, astro-ph/0512416
Zappacosta, L., Buote, D. A., Gastaldello, F., Humphrey, P. J., Bullock, J. S., Brighenti, F., & Mathews, W. G. 2006, ApJ, submitted, astro-ph/0602613
Zentner, A. R., Berlind, A. A., Bullock, J. S., Kravtsov, A. V., & Wechsler, R. H. 2005, ApJ, 624, 505
Zentner, A. R. & Bullock, J. S. 2002, Phys. Rev. D, 66, 043003
Zezas, A., Birkinshaw, M., Worrall, D. M., Peters, A., & Fabbiano, G. 2005, ApJ, 627, 711